

156
65

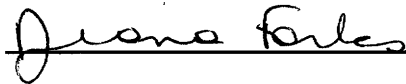
Computer Simulation Study of Grain Boundary Structure in B2 NiAl

by

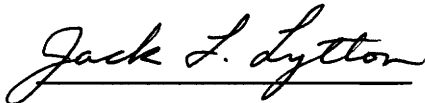
Guy J. Petton

dissertation submitted to the Faculty of the
Virginia Polytechnic Institute and State University
in Partial fulfillment of the requirements for the degree of
Master of Science
in Materials Engineering

APPROVED:



Diana Farkas, Chairperson



Jack L. Lytton



Robert W. Hendricks

September 19, 1990

Blacksburg, Virginia

L5
5055
V855
1910

P453
C.2

Computer Simulation Study of Grain Boundary Structure in B2 NiAl

by

Guy J. Petton

Diana Farkas, chairperson

Materials Engineering

(ABSTRACT)

In an effort to understand intrinsic grain boundary brittleness, computer simulation of grain boundary structures in ordered NiAl was carried out. The considered boundaries were boundaries of low reciprocal coincident site density Σ . The structural unit model was used to obtain a general picture of the grain boundary features in NiAl. Relation between the grain boundary stoichiometry and the energy was studied and it was found that the grain boundary energy increases with a higher aluminum content in the grain boundary. Thus, excess of aluminum in the grain boundary seems to make the material brittle. The grain boundaries obtained are relatively dense and grain boundary brittleness would not be expected to originate from large interstitial holes. However, the structures computed show a large spread in energy values and it is proposed that the observed brittleness is due to the appearance of high energy structures when dislocations arrive at the boundary.

ACKNOWLEDGEMENTS

The author wishes to acknowledge the committee chairperson Dr Diana Farkas for her great help in understanding the problem and handling the results during innumerable informal discussions. The author wants also to acknowledge his committee members Dr Jack Lytton and Dr Robert Hendricks. The support and advice from Dr Robert Hendricks and especially at the arrival in Virginia Tech were primordial in the accomplishment of the Master program. Benefits from the courses taught by Dr Jack Lytton were useful in the course of this study. The author wants to thank Dr A. Voter who provided the interatomic potentials used in this study. The author wishes to thank the members of the laboratory Antonio Cardozo, Zhaoyang Xie and Jun Liao for the good atmosphere they brought and also Dr Roberto Pasianot and Dr Ho Jang for their help and suggestions. The author thanks above all his wife Bénédicte without her support and encouragement nothing would have been possible.

This work was sponsored by the Office of Naval Research, Division of Materials Science.

TABLE OF CONTENTS

1 INTRODUCTION.....	1
2 THEORY OF GRAIN BOUNDARY GEOMETRY.....	4
2.1 Crystal Structure of NiAl.....	4
2.2 Grain Boundary Structure.....	6
3 COMPUTER SIMULATION TECHNIQUE.....	13
3.1 General Overview.....	13
3.1.1 Analytical Method.....	14
3.1.2 Solution for Planar Defects.....	16
3.1.3 Numerical Methods.....	16
3.2 Interatomic Potentials.....	18

3.2.1	Pair potentials.....	18
3.2.2	Local Volume dependent potentials.....	20
3.2.3	Grain Boundary Cohesion.....	21
3.3	Simulation Procedure.....	22
3.3.1	Perfect Lattice Generation.....	22
3.3.2	Generation of Grain Boundary.....	23
3.3.3	Energy Minimization Procedure.....	24
3.3.4	General Procedure.....	25
4	RESULTS.....	27
4.1	[001] Symmetrical Tilt Boundaries.....	28
4.1.1	$\Sigma = 5(210)$ Symmetrical Tilt Boundary	28
4.1.1.1	Stoichiometric $\Sigma = 5(210)$ Grain Boundary Structures (Figures (4-14)).....	29
4.1.1.2	One atom rich $\Sigma = 5(210)$ Grain Boundary Structures (Figures (15-32)).....	41
4.1.1.3	Two atoms rich $\Sigma = 5(210)$ Grain Boundary Structures (Figures (33-35)).....	60
4.1.2	$\Sigma = 5(310)$ Symmetrical Tilt Boundary	65
4.1.3	$\Sigma = 29(520)$ Symmetrical Tilt Boundary	65
4.1.4	General Results.....	82
4.2	$\Sigma = 3(11\bar{2})[1\bar{1}0]$ Tilt Boundary.....	90
5	DISCUSSION.....	97

6 CONCLUSIONS.....	108
7 REFERENCES.....	110
VITA.....	114

LIST OF ILLUSTRATIONS

Figure 1	Crystal structure of NiAl.....	5
Figure 2	Coincidence site lattice for (210) symmetric tilt boundary.....	7
Figure 3	Coincidence site lattice for (210) twist boundary.....	9
Figure 4	Stoichiometric $\Sigma = 5(210)$ grain boundary structure.....	30
Figure 5	Stoichiometric $\Sigma = 5(210)$ grain boundary structure.....	31
Figure 6	Stoichiometric $\Sigma = 5(210)$ grain boundary structure.....	32
Figure 7	Stoichiometric $\Sigma = 5(210)$ grain boundary structure.....	33
Figure 8	Stoichiometric $\Sigma = 5(210)$ grain boundary structure.....	34
Figure 9	Stoichiometric $\Sigma = 5(210)$ grain boundary structure.....	35
Figure 10	Stoichiometric $\Sigma = 5(210)$ grain boundary structure.....	36
Figure 11	Stoichiometric $\Sigma = 5(210)$ grain boundary structure.....	37
Figure 12	Stoichiometric $\Sigma = 5(210)$ grain boundary structure.....	38

Figure 13	Stoichiometric $\Sigma = 5(210)$ grain boundary structure.....	39
Figure 14	Stoichiometric $\Sigma = 5(210)$ grain boundary structure.....	40
Figure 15	One excess Ni atom $\Sigma = 5(210)$ grain boundary structure.....	42
Figure 16	One excess Ni atom $\Sigma = 5(210)$ grain boundary structure.....	43
Figure 17	One excess Ni atom $\Sigma = 5(210)$ grain boundary structure.....	44
Figure 18	One excess Ni atom $\Sigma = 5(210)$ grain boundary structure.....	45
Figure 19	One excess Ni atom $\Sigma = 5(210)$ grain boundary structure.....	46
Figure 20	One excess Ni atom $\Sigma = 5(210)$ grain boundary structure.....	47
Figure 21	One excess Ni atom $\Sigma = 5(210)$ grain boundary structure.....	48
Figure 22	One excess Ni atom $\Sigma = 5(210)$ grain boundary structure.....	49
Figure 23	One excess Ni atom $\Sigma = 5(210)$ grain boundary structure.....	50
Figure 24	One excess Al atom $\Sigma = 5(210)$ grain boundary structure.....	51
Figure 25	One excess Al atom $\Sigma = 5(210)$ grain boundary structure.....	52
Figure 26	One excess Al atom $\Sigma = 5(210)$ grain boundary structure.....	53
Figure 27	One excess Al atom $\Sigma = 5(210)$ grain boundary structure.....	54
Figure 28	One excess Al atom $\Sigma = 5(210)$ grain boundary structure.....	55
Figure 29	One excess Al atom $\Sigma = 5(210)$ grain boundary structure.....	56
Figure 30	One excess Al atom $\Sigma = 5(210)$ grain boundary structure.....	57
Figure 31	One excess Al atom $\Sigma = 5(210)$ grain boundary structure.....	58
Figure 32	One excess Al atom $\Sigma = 5(210)$ grain boundary structure.....	59
Figure 33	Two excess Ni atoms $\Sigma = 5(210)$ grain boundary structure.....	60
Figure 34	Two excess Ni atoms $\Sigma = 5(210)$ grain boundary structure.....	62
Figure 35	Two excess Al atoms $\Sigma = 5(210)$ grain boundary structure.....	63

Figure 36	Grain boundary energy as a function of excess in aluminum for $\Sigma = 5(210)$ grain boundary structures.....	64
Figure 37	Stoichiometric $\Sigma = 5(310)$ grain boundary structure.....	66
Figure 38	Stoichiometric $\Sigma = 5(310)$ grain boundary structure.....	67
Figure 39	Stoichiometric $\Sigma = 5(310)$ grain boundary structure.....	68
Figure 40	Stoichiometric $\Sigma = 5(310)$ grain boundary structure.....	69
Figure 41	Stoichiometric $\Sigma = 5(310)$ grain boundary structure.....	70
Figure 42	Stoichiometric $\Sigma = 5(310)$ grain boundary structure.....	71
Figure 43	Stoichiometric $\Sigma = 5(310)$ grain boundary structure.....	72
Figure 44	Stoichiometric $\Sigma = 5(310)$ grain boundary structure.....	73
Figure 45	Stoichiometric $\Sigma = 5(310)$ grain boundary structure.....	74
Figure 46	Stoichiometric $\Sigma = 29(520)$ grain boundary structure.....	75
Figure 47	Stoichiometric $\Sigma = 29(520)$ grain boundary structure.....	76
Figure 48	One excess Al atom $\Sigma = 29(520)$ grain boundary structure.....	77
Figure 49	One excess Ni atom $\Sigma = 29(520)$ grain boundary structure.....	78
Figure 50	Stoichiometric $\Sigma = 29(520)$ grain boundary structure.....	79
Figure 51	Stoichiometric $\Sigma = 29(520)$ grain boundary structure.....	80
Figure 52	One excess Ni atom $\Sigma = 29(520)$ grain boundary structure.....	81
Figure 53	d as a function of the tilt angle θ	84
Figure 54	Definition of d_1 and d_2	85
Figure 55	d_1 as a function of the grain boundary energy.....	86
Figure 56	d_1 as a function of the equilibrium shift perpendicular to the grain boundary plane (excess volume).....	87
Figure 57	d_2 as a function of the grain boundary energy.....	88

Figure 58	d_2 as a function of the equilibrium shift perpendicular to the grain boundary plane (excess volume).....	89
Figure 59	Stoichiometric $\Sigma = 3(11\bar{2})$ grain boundary structure.....	93
Figure 60	Stoichiometric $\Sigma = 3(11\bar{2})$ grain boundary structure.....	94
Figure 61	Stoichiometric $\Sigma = 3(11\bar{2})$ grain boundary structure.....	95
Figure 62	Stoichiometric $\Sigma = 3(11\bar{2})$ grain boundary structure.....	96
Figure 63.	Influence of the atoms in the structural unit $\Sigma = 5(210)$ grain boundary structures.....	99
Figure 64.	Configuration of lowest energy for $\Sigma = 5(210)$ grain boundary structures.....	102
Figure 65.	Features of the favored boundaries.....	104
Figure 66.	Features of the favored boundaries.....	105
Figure 67.	Features of the favored boundaries.....	106

LIST OF TABLES

Table 1	Distance d between the nearest layers after relaxation for $[001]$ tilt boundaries in the case of no interchanging in atom types, no shift in Z and no layer taken out.....	83
Table 2	Distance d_1 between the grain boundary and the next nearest layer before relaxation, and the Rigid Body Translation perpendicular to the Grain Boundary plane (excess volume) and the Grain Boundary Energy in the case of no interchanging in atom types, no shift in Z and no layer taken out.....	91
Table 3	Distance d_2 between the grain boundary and the next nearest layer before relaxation, and the Rigid Body Translation perpendicular to the Grain Boundary plane (excess volume) and the Grain Boundary Energy in the case of no interchanging in atom types, no shift in Z and the first layer taken out.....	92

1 INTRODUCTION

There has been a growing interest over the last decades in ordered alloys for their potential use as high temperature materials. Especially, nickel aluminum alloys appear to be of multiple applications. As a matter of fact, Ni₃Al L1₂ structure exhibits an increasing yield strength with temperature up to 600°C [1], and NiAl B2 phase has even a higher yield strength than Ni₃Al [2]. However, grain boundary embrittlement has been a major problem. Indeed, even if single crystals show ductility, polycrystalline materials are brittle. This lack of ductility prohibits the practical application of these materials as high temperature corrosion resistant structural alloys.

Also, grain boundaries have received a substantial experimental and theoretical attention in order to develop a better understanding of the structures and energetic phenomena. In this study, the $\Sigma = 5(210)$ and $\Sigma = 5(310)[001]$ tilt boundaries were exhaustively studied in the NiAl B2 phase where the parameter called Σ is the reciprocal coincident site density,

which means the lower the Σ , the more numerous the sites in coincidence between the two crystals across the boundary. These boundaries present a particular interest because they exhibit a low reciprocal coincident site density Σ and relatively low energies. These boundaries are called favored boundaries. Another interesting feature is that results obtained for favored boundaries may be extended to non-favored boundaries in the nearby misorientation using the "structural unit" model [3,4,5].

According to experimental work [2,6] and computer simulation results [7], grain boundary stoichiometry has an important effect on the intergranular brittleness and the yield strength in the case of Ni₃Al. Recently, the relationship was also experimentally exhibited in the NiAl B2 phase [2]. Then, different boundary stoichiometries were computed for the $\Sigma = 5(210)$ boundary. We considered only the stoichiometric boundaries for the $\Sigma = 5(310)$ boundary.

Some configurations of the non-favored $\Sigma = 29(520) [001]$ tilt boundaries were also studied. As the misorientation of the $\Sigma = 29(520)$ non-favored boundary falls within the misorientation of both $\Sigma = 5(210)$ and $\Sigma = 5(310)$ favored boundaries (Table 1), confirmation of the properties of the favored boundaries can be retrieved.

In the case of Ni₃Al (L₁₂ structure), the positions of atoms at the grain boundary appear to be asymmetric in most boundaries [8,9]. The asymmetry of the boundary, which means the presence of large interstitial holes, was assumed to be the reason for the brittleness [7]. The intergranular brittleness of the Ni₃Al L₁₂ compound was found to be intrinsic to the structure of the material [7]. The $\Sigma = 3$ boundaries were found to be an exception and experimental work also concluded that these boundaries were avoided by the cracks during the fracture process [10,11].

As the purpose of this work is contribute to the understanding of the intergranular brittleness of NiAl B2 ordered material, the grain boundary structures and energies are the features to be observed. An interesting result is to know if the interpretation of intrinsic brittleness found in the case of Ni₃Al L₁₂ structure still applies for B2 ordered NiAl. In addition, by systematically studying particular boundaries such as $\Sigma = 5(210)$ and $\Sigma = 5(310)$, trends

may be evidenced. These trends will allow the prediction of the structures and the range of energies of non studied boundaries, and will give a general picture of the features relative to grain boundaries in NiAl.

To study the above-mentioned grain boundaries, we used the technique of computer simulation [4], which essentially consists of a numerical method, called conjugate gradients, to minimize the energy of an ensemble of atoms, once the interaction law is given. This latter is the embedded atom method (EAM) potential which includes a local volume term besides a pair interaction term [12].

The concept of the coincident site lattice (CSL) based on the interpenetration of two relatively misoriented crystals (for a review see for instance Refs 3 and 13) is used throughout the work.

At first, geometry of the grain boundary is overviewed in section 2 and the basis of the computer simulation technique in section 3. Then, the results are presented in section 4. Finally, we present the discussion and conclusion in sections 5 and 6, respectively.

2 THEORY OF GRAIN BOUNDARY GEOMETRY

2.1 Crystal structure of NiAl

In ordered alloys the probability of an atom of a certain type to occupy a specific site inside the lattice is higher than for some other sites, contrary to disordered alloys in which a random distribution is observed. The resultant lattice structure of ordered alloys can be seen as the interpenetration of two lattices, each one corresponding to an atom type, nickel or aluminum in the case of NiAl.

The structure of the ordered alloy NiAl is the B2 structure which is very similar to the bcc for a pure material. The B2 cell corresponds to a bcc cell with an atom type at the corner cube positions and the other atom type in the center of the cube (see Figure (1)). Both atom

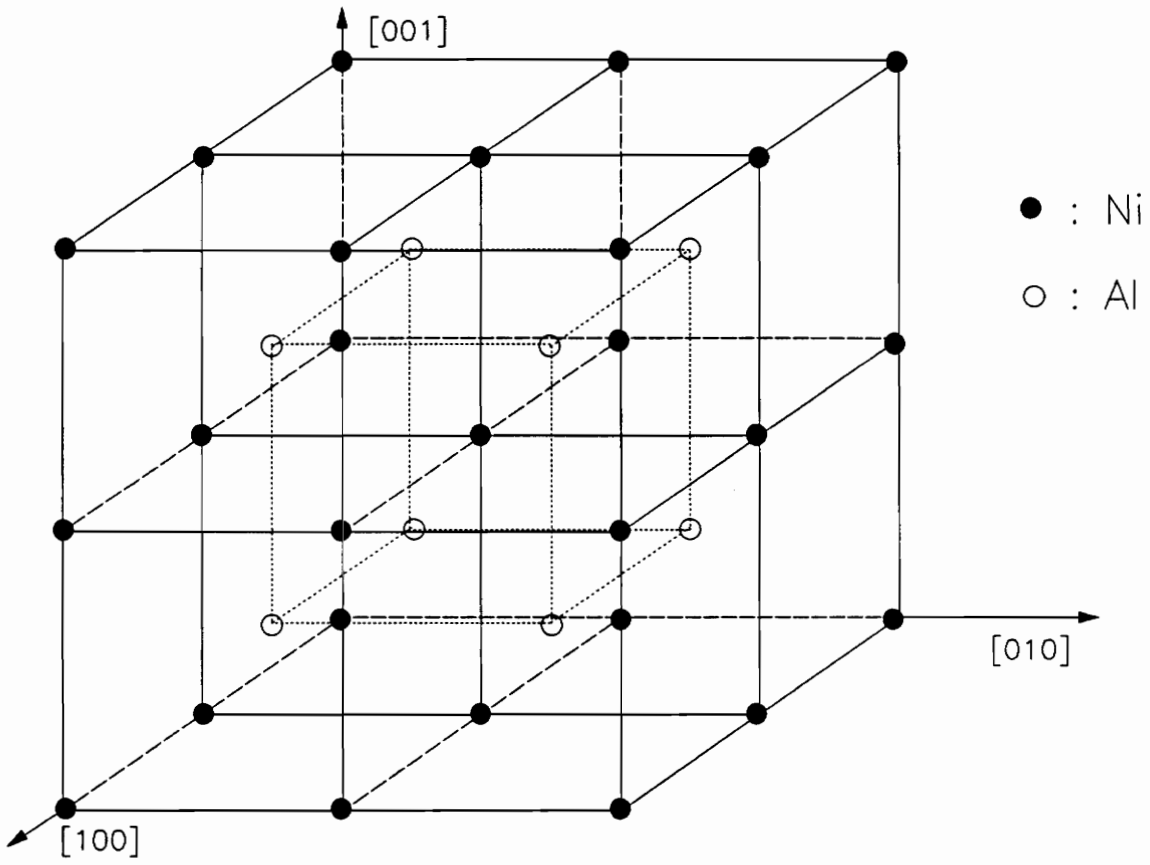


Figure 1. Crystal structure of NiAl

types play the exact same role inside the lattice. Indeed, interchanging the atom types rebuilds the B2 phase. The interchanging corresponds to a $\frac{1}{2}a_0[111]$ translation of the whole perfect lattice, with a_0 the lattice parameter ($a_0 = 2.87 \text{ \AA}$).

2.2 Grain boundary structure

Grain boundaries were first thought as amorphous areas as no actual means existed to study their structures. Since then, several techniques have been developed and theories have been set up in order to understand the observed mechanical and kinetic properties of the grain boundaries. The coincidence site lattice theory is one of these models, commonly accepted and used, and summarized below.

The grain boundary is often described as a planar interface between two crystals which mismatch due to a misorientation or a mistranslation. There are two particular types boundaries, namely the rotational axis which yields the misorientation is either parallel or perpendicular to the grain boundary. They are called respectively tilt and twist boundaries.

The **twist boundaries** can be viewed as a cross grid of pure screw dislocations with dislocation lines in the boundary plane [14]. An angle is defined between a same family of planes in the two crystals, the twist angle.

The **tilt boundaries** are also seen as an array of edge dislocation of the same Burgers vector and of parallel dislocation lines in the same plane [14]. The Burgers vector is then normal to the boundary plane. The misorientation angle is called now the tilt angle. When the grain boundary plane bisects the tilt angle, a very special boundary is obtained called **symmetric tilt boundary** (Figure (2)). Only symmetrical tilt boundary are considered in this study.

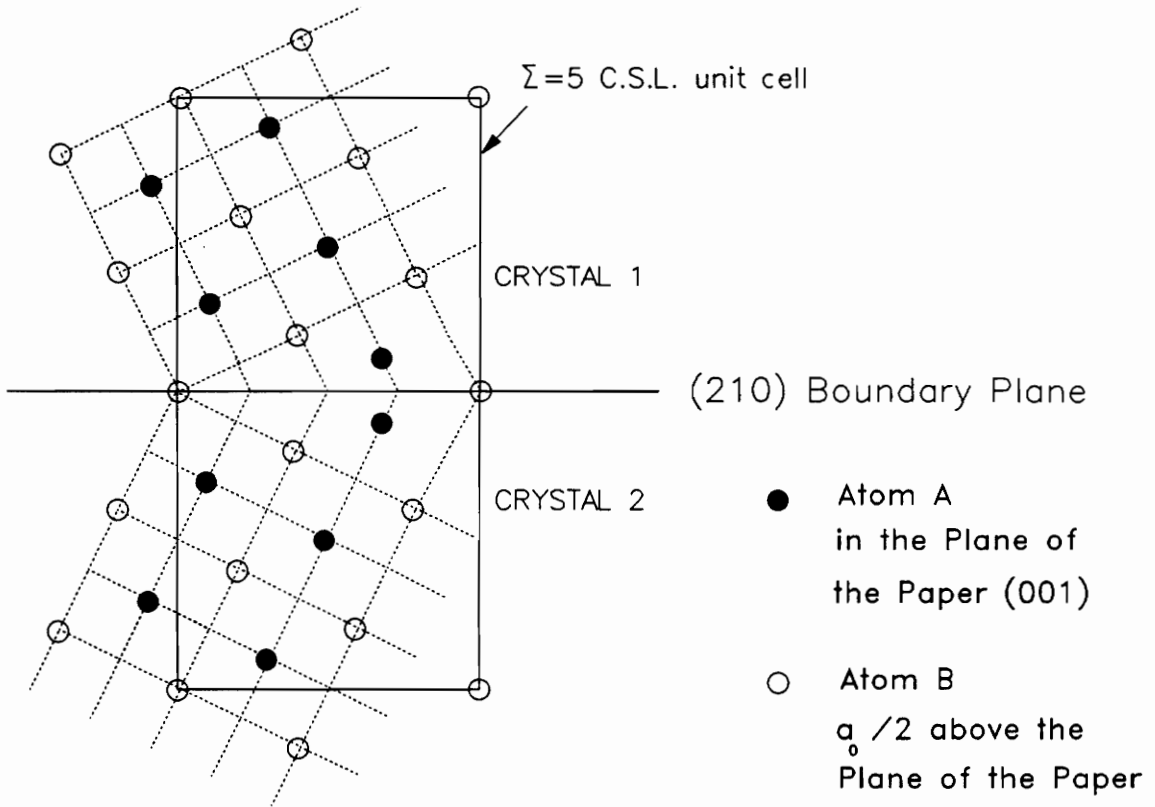


Figure 2. Coincidence site lattice for (210) symmetric tilt boundary

In order to characterize a boundary, five macroscopic parameters exist. Two of those are for directions of the boundary plane, the three remaining parameters for the relative misorientation of the crystals across the boundary. Then, four more microscopic parameters are needed. Three of those correspond to the relative shift of one crystal with respect to the other. The last one allows a degree of freedom for the boundary plane to be shifted parallel to itself.

Coincidence Site Lattice Theory

The coincidence site lattice (CSL) theory (see for review refs 4 and 13) is a very popular model for the characterization of grain boundaries. The model has met with considerable success in the case of the equilibrium structure of grain boundaries for cubic materials. Because features of the CSL model are used in this study, its main points are summarized here.

The coincident site lattice is the result of interpenetrating lattices of two crystals giving rise to a superlattice. If one site of both crystals is brought into coincidence and then a relative rotation is applied, may result in a relative misorientation called coincidence orientation. The sites which belong to both crystals are the coincident sites and form the coincident site Lattice. The concept is visualized in Figures 2 and 3 for tilt and twist boundary respectively.

The reciprocal coincident site density denoted as Σ is also used to characterize the boundaries. For example, $\Sigma = 5$ means that one in every five atoms is coincident. So, the higher the Σ , the less numerous the coincident sites. As a matter of fact, for $\Sigma = 1$ there is no boundary at all.

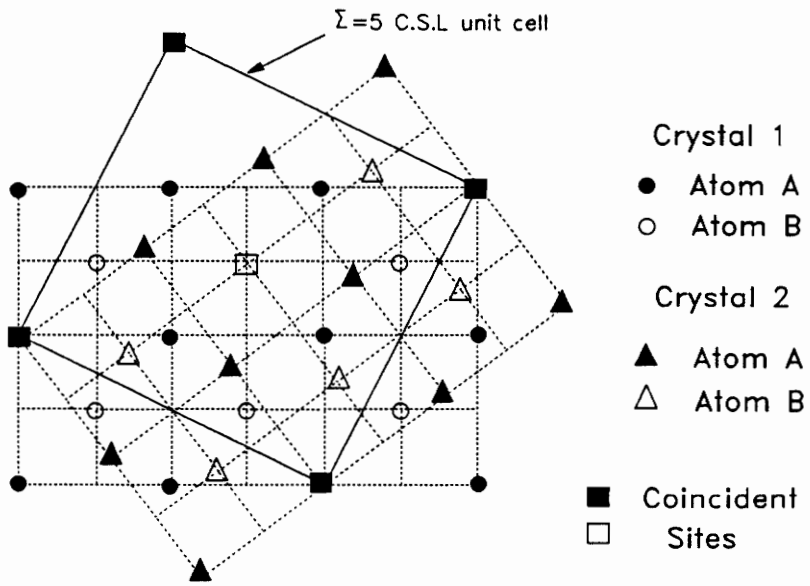


Figure 3. Coincidence site lattice for (210) twist boundary

A two-dimensionally periodic structure can be found for all CSL boundaries if the two crystals are thought of as interpenetrating. This periodicity is conserved in the actual bicrystal for the the directions contained in the grain boundary plane. The two dimensional repeat cells are called structural units. The size of the structural unit is a function of the reciprocal density of coincident sites Σ [3]. Structural units of particular boundaries called the favored boundaries may be found as the structure elements of non-favored boundaries [3,4,5]. Favored boundaries are usually short period boundaries, and structural units of these special boundaries are found to be fundamental units of longer period boundaries in the nearby misorientation. As a matter of fact, as the size of the structural unit appears to be related to Σ , favored boundaries are found to be usually associated with low Σ . From a statistical point of view, the favored boundaries appear to be more frequent than the non-favored ones [15]. According to Sutton and Vitek [3], the atomic structure and the stress field of any non-favored boundary within the misorientation of two favored boundaries can be predicted using the features of the same favored boundaries.

Computer simulations using CSL theory [7] have shown that favored boundaries usually exhibit low grain boundary energy. Also, the CSL model brought about a satisfactory interpretation of experimental results. Indeed, cusps were observed in grain boundary energy versus crystals misorientation plots [16,17]. These cusps correspond to high density CSL boundaries.

When the crystal misorientation of the two adjoining crystals deviates from the high density CSL misorientation (low Σ), a network of grain boundary dislocations (GBD) appears in order to compensate for the deviation. The grain boundary becomes a network of dislocations embedded in a low energy, high density CSL interface [18]. For favored boundaries the long-range elastic stress fields of the dislocations cancel. The Burgers vectors of the dislocations are usually vectors of the displacement shift complete (DSC) lattice which is the lattice of displacements of lattice 2 with respect to lattice 1 that causes shifts of the complete pattern of coincident site lattice. In other words, two interpenetrating lattices at some coincidence orientation may be translated one with respect to the other by a vector \vec{t} and the pattern will be reconstructed again. The vector \vec{t} is a vector joining lattice points from either of the crystal

lattices in the coincidence orientation [4]. The new CSL resulting from this translation can also be rotated with respect to the original unit cell. All these displacements constitute the DSC lattice which corresponds to the CSL .

In order to describe high angle boundaries, the dislocation model of grain boundaries has to be introduced. The dislocation model has suggested that a net Burgers vector B may be defined. B is the Burgers vector of interfacial dislocations crossing any given vector \vec{p} in the interface, and S_i ($i=1,2$) the lattice deformation producing lattice "i" from a reference lattice S , the Frank-Bilby equation (Frank 1950, Bilby 1955) is written

$$B = (S_2^{-1} - S_1^{-1})p$$

S_1 and S_2 can be replaced by U_1S_1 and U_2S_2 where U_1 and U_2 are lattice-invariant deformations which have the effect of shearing the two crystals into themselves resulting in no change in either them or the interface [3]. The net Burgers vector B depends on the choice of S_1 and S_2 , leading to an infinite manifold of descriptions for a given interface and reference lattice. If lattices match perfectly at the interface, the boundary plane is in fact an invariant plane of simple shear. In that case, there is no dislocation in the boundary. The boundary in a twin deformation can be seen as a plane of simple shear for which the reference structure is either an ideal lattice or a special boundary. The Burgers vectors of the GBD for the ideal lattice are those of the lattice dislocations and for special boundaries of the DSC lattice associated with the corresponding CSL . Finally, a high angle boundary has a dislocation content of a set of primary dislocations associated with the special boundary and a set of secondary dislocations associated with the DSC lattice. The secondary dislocations compensate for the deviation from the structure of the special boundary.

According to Brokman and Balluffi [19], the construction of the grain boundary may be described in terms of three steps.

- 1 At first, lattice 1 and 2 are brought together in order to form the boundary. All atoms of both crystals are held rigidly in their perfect lattice positions. Lattice 2 is translated with respect to lattice 1 in order to achieve the minimum energy. In general, lattices are misoriented by the angle θ to create the CSL.
- 2 Then, primary relaxations occur in some regions of the boundary. The regions are centered on elements of an appropriately chosen O-Lattice as described by Bollmann [13]. These relaxations allow local matching across the boundary.
- 3 Finally, secondary relaxations occur in high Σ boundaries in order to produce the secondary grain boundary dislocation network that allows deviation from nearby low Σ misorientations.

3 COMPUTER SIMULATION TECHNIQUE

3.1 General Overview

The displacements of atoms around the defects may be analytically or numerically computed. The first method becomes rapidly complex with the size of the problem and is almost untreatable without the help of some approximation, like the harmonic approximation. Indeed, huge matrices have to be handled as the interaction between all the atoms must be considered,

even though the symmetries of the ordered alloys are used. However, the analytical method has to be understood since it is fundamental for the calculation of the displacements of the atoms around the defect.

3.1.1 Analytical method

Let Φ be the total energy at any time and u_i an infinitesimal displacement of an atom in the direction i . If a number, m , of atoms is moved in the direction i the negative force acting on the atoms at the equilibrium position is written

$$F_i = - \frac{\partial \Phi}{\partial u_i(m)} \quad (3.1)$$

Then, moving the m' atom in the direction j induces the force on the m atom atoms parallel to the direction i

$$F_{ij}(m, m') = - \frac{\partial^2 \Phi}{\partial u_i(m) \partial u_j(m')} \quad (3.2)$$

The left terms in equation (3.2) are called **atomic force constants** and they yield the force constant matrix which is of rank $3 \times N$ by $3 \times N$, where N is the total number of atoms in the crystal. Calling Φ_0 the equilibrium energy, the total energy Φ may be expanded using the Taylor series expansion

$$\Phi = \Phi_0 + \sum_m F_i(m) u_i(m) + \frac{1}{2} \sum_m \sum_{m'} F_{ij}(m, m') u_i(m) u_j(m') +$$

$$\frac{1}{6} \sum_m \sum_{m'} \sum_{m''} \Phi_{ijk}(m, m', m'') u_i(m) u_j(m') u_k(m'') + \dots \quad (3.3)$$

In expression (3.3) if the terms above the second order of the Taylor series expansion are neglected the approximation is known as the **harmonic approximation** of the potential energy.

$$\Phi = \Phi_0 + \sum_m \Phi_i(m) + \frac{1}{2} \sum_m \sum_{m'} \Phi_{ij}(m, m') u_i(m) u_j(m') \quad (3.4)$$

As, at the equilibrium positions forces becomes nul

$$\Phi_i(m) = 0 \quad (3.5)$$

equation (3.4) may be differentiated using (3.5)

$$\sum_{m'} \Phi_{ij}(m, m') u_j(m') = F_i(m) \quad (3.6)$$

and finally, using mathematical tools for matrix inversion

$$u_j(m') = \sum_{im} G_{ji}(m', m) F_i(m) \quad (3.7)$$

where G_{ji} is a tensor known as the Green's Function [20]. It is the inverse of the force constant matrix. This expression (3.7) is very useful in the calculation of the atomic displacements $u_j(m')$ around a defect.

3.1.2 Solution for Planar Defects

These relations applied to a strong defect, such as a grain boundary, may show much inaccuracy close to the defect. Indeed, even the Kanzaki force $K_i(m)$, which includes a correction to forces due to anharmonic terms

$$K_i(m) = \sum_{m'} \Phi_{ij}(m, m') u_j(m') \quad (3.8)$$

$$K_i(m) = F_i(m) - \sum_{m'} \Delta \Phi_j(m, m') u_j(m') \quad (3.9)$$

becomes more precise when measurements are done far from the defect. So, an accurate enough estimation of the defect effects may be obtained using the Kanzaki force only for atoms in an area far from the defect. Thus, although the Kanzaki force is not useful for atomic displacements around grain boundaries, it may be used for other studies about planar defects such as oscillation modes [21]. So, more precise methods are needed and the numerical methods is one of those.

3.1.3 Numerical Methods

Since long ago, numerical relaxation techniques have been set up and widely used in order to predict the atomistic configuration around defects. These techniques were particularly useful for strong defects such as grain boundaries. Many computer codes have been developed to deal with the problem, among them the DEVIL code [22], a version of which is used in this study. The main steps of the computer code can be sketched as

- 1) the perfect lattice is first generated,
- 2) the defect is introduced, and finally
- 3) the relaxation around the defect is allowed.

Every atom located in a three dimensional lattice is allowed to interact with all its neighboring atoms according to some interaction potential (see chapter 3.2). The sum of the interactions is the total energy of the crystal. The presence of the defect induces forces on the crystal atoms that drive the system to a new equilibrium configuration corresponding to a minimum in the energy of the defect lattice.

The conjugate gradient method is used to accomplish the relaxation. This technique consists of moving the atomic coordinates in a $3 \times N$ dimensional space, choosing successive "conjugate" directions (perpendicular to the previous one) and minimizing the energy of the system in each direction chosen. The process is continued until the forces on each atom are below a certain small selected value. The first direction is the steepest descent direction. This is the direction in which the rate of energy decrease is maximum. The conjugate gradient method is known as a fast convergent technique for big problems.

3.2 Interatomic potentials

3.2.1 Pair potentials

The advent of fast and large storage computers of the last decades, has allowed the researchers to apply computer simulation to complex defect structures. At the same time physically more realistic potentials have become available, widening the scope of the field. Then, it is obvious that the type of interatomic potential used for the computation has a strong influence on the results. At the beginning, most calculations were carried out with the so-called pair potentials [23].

A two body interatomic potential is a potential which describes the interaction as a function of the distance. Usually, as the two atoms are brought closer they attract each other till the minimum energy distance is reached. Beyond this point, they repel, and all the more as they come closer. Within this scheme, the energy of the crystal is written as :

$$E = \frac{1}{2} \sum_i \sum_{i \neq j} \Phi(r_{ij}) \quad (3.10)$$

where E is the total energy of the system, r_{ij} the distance between atoms i and j , and Φ a pairwise interatomic potential.

Many forms were developed for the term Φ . And for each form, several experimental data might be used in order to fit the potentials. However, all potentials must fit both the lattice parameter and the cohesive energy of the most common stable phase. A very popular potential is the Lennard-Jones potential which includes both repulsive and attractive parts of the interatomic field. The Lennard-Jones potential was most commonly used under the form [23]

$$\Phi(r_{ij}) = \frac{A}{r_{ij}^n} - \frac{B}{r_{ij}^m} \quad (3.11)$$

where usually $n=12$ and $m=6$.

These three conditions have to be satisfied by all potentials :

- * $\Phi(r_{ij}) \rightarrow 0$ as $r \rightarrow \infty$
- * $\Phi(r_{ij})$ has a minimum for $r = r_0$ (intermolecular separation)
- * $\Phi(r_{ij}) \rightarrow \infty$ as $r \rightarrow 0$

Morse first imposed another condition on the potential which is to fit vibrational spectra of the molecules. Then, he proposed this form [23]

$$\Phi(r_{ij}) = D e^{-2\alpha(r_{ij}-r_0)} - 2D e^{-\alpha(r_{ij}-r_0)} \quad (3.12)$$

where D and α are the new parameters used to fit the essential constants of the material. However these potentials fail to produce the elastic properties of the material. More accurate potentials will be developed (see 3.2.2).

In the case of alloys, Machlin has proposed a successful scheme [24,25,26]. In an alloy AB, potentials for pure A and pure B are determined using standard fitting procedures, and the average of these two potentials is taken as being the one of the alloy. Another term is added as needed to fit lattice parameter, cohesive energy and charge transfer.

However, as the cohesive energy in metals is mainly due to an electron cloud, it seems necessary to add to the previous sorts of potentials, a local volume-dependent term which may describe the electronic density.

3.2.2 Local Volume dependent potentials

Adding a local volume-dependent term has been shown to be an improvement over simple pair interactions [27]. Equilibrium pair potentials are unable to fit all the elastic constants of the material and the vacancy formation energy is always almost the same as the cohesive energy. This is no more the case for the class of potentials described here.

A particularly important feature is that these potentials come closer to reality when describing surface relaxations [27], for which pair potentials were even qualitatively wrong.

The total energy of the crystal is now given by

$$E = \frac{1}{2} \sum_i \sum_{j \neq i} [\Phi(r_{ij}) + U_{ij}(V)] \quad (3.13)$$

where Φ is a pair term like in equation (3.10) and $U_{ij}(V)$ is the volume dependent term. We may use the same scheme as seen for pairwise potentials [24,25,26] to extend the potential to alloys [28]. An improved form of the volume dependent potential is the embedded atom type, which is used in this study. For the embedded atom potential the volume dependent term $U_{ij}(V)$ is based on the local electronic density and the total energy of the crystal may be written

$$E = \sum_i E_i \quad (3.14)$$

with the term E_i which is the contribution to the energy of atom "i", namely

$$E_i = \frac{1}{2} \sum_{j \neq i} \Phi(r_{ij}) + F(\rho_i) \quad (3.15)$$

where ρ_i is written

$$\rho_i = \sum_{j \neq i} \rho(r_{ij}) \quad (3.16)$$

and can be interpreted as the local electronic density at atomic site "i" due to all its neighbors. There are now two terms included in the total energy. The pairwise one which corresponds to the electrostatic interaction between atoms, and the new one $F(\rho_i)$ which may be seen as the embedded energy of the atom "i" in an electron gas of density ρ_i . In this study, the interatomic potential deduced by Voter and Chen is used for the calculation [12]. It is an embedded atom type of potential.

3.2.3 Grain Boundary Cohesion

The grain boundary energy, γ_{gb} , is the difference between the total energy of the crystal with the defect, E_{def} , and the total energy of the perfect crystal, E_{perf} :

$$\gamma_{gb} = E_{def} - E_{perf} \quad (3.17)$$

Then, since two free surfaces are created (S_1 and S_2) and the grain boundary is destroyed, the grain boundary cohesive energy, γ_{coh} , is defined as

$$\gamma_{coh} = \gamma_{S_1} + \gamma_{S_2} - \gamma_{gb} \quad (3.18)$$

Thus, the grain boundary energy and the grain boundary cohesive energy are inversely related. The higher the grain boundary energy, the lower the grain boundary cohesive energy, and the easier the fracture.

3.3 Simulation procedure

3.3.1 Perfect Lattice Generation

The crystal structure is generated on the base of information regarding the unit cell. In the case of the B2 structure, nickel is stated to be at (000) and aluminum at $(\frac{1}{2}\frac{1}{2}\frac{1}{2})$. The perfect lattice is created by repeating the original unit cell along the cartesian directions X, Y and Z, leading to the relation between the vector of coordinates of the atom M, $S[M]$, and the one of atom M_0 , $S[M_0]$ (with M_0 , atom of the original unit cell)

$$S[M] = S[M_0] + m \delta x \bar{X} + n \delta y \bar{Y} + o \delta z \bar{Z} \quad (3.17)$$

with m, n and o integers and δx , δy and δz the periodic lengths.

Then, a limiting block is defined inside which all atoms are located. This block is a parallelepiped, the sides of which being planes whose normals are paralel to X, Y and Z.

All atoms inside this block are allowed to move freely according to the interactions defined by the potential. Atoms located at the block surface loose interactions due to the lack of neighbors. In order to prevent this situation, an outer block, Region II, that embeds the first, is created. The atoms in Region II are only under the influence of the long range elastic fields of the defect. The relaxation is not applied in this region.

Throughout the study Y is the axis perpendicular to the grain boundary defined by X and Z. Thus, periodic boundary conditions may be used along X and Z axis. This allows the program to handle less atoms in Region I, as it can take only one period in X and Z directions. For our study of grain boundaries, fixed boundary conditions (Region II) are encountered in the Y direction.

3.3.2 Generation of grain boundary

In order to generate a grain boundary, an angle and a rotation axis must be defined. Since there are 48 rotation symmetry operations in the cubic group, a misorientation of two cubic crystals may be given by 24 different angle/rotation axis. So, for each value of Σ there are 24 angle/rotation axis couples [15].

In our case, the rotation axis is the tilt axis and the angle the tilt angle of the corresponding CSL (see values in Table 1 page 83). Because the studied boundaries are symmetrical tilt boundaries, the boundaries have been constructed by changing X to $-X$ in one crystal. This corresponds to the building of a mirror image about the (Y,Z) plane.

Three main modifications may be brought to the initial unrelaxed grain boundary leading to different possible configurations.

- 1 Taking layers out which creates structural vacancies in the vicinity of the grain boundary yielding structures with excess nickel or aluminum,
- 2 Interchanging atom types in one of the crystals which locates nickel and aluminum atoms "in front of" each other. This corresponds to shifting one crystal by $\frac{1}{2}a_0[101]$,
- 3 Shifting one crystal with respect to the other by $\frac{1}{2}a_0$ along Z , or
- 4 moving the grain boundary plane parallel to itself resulting in a grain boundary plane content of either nickel or aluminum.

All combinations of these modifications may be made. A last modification which does not change the structure is the translation along Y.

Indeed, the crystals must be taken apart along Y in order to find the position for which the grain boundary energy becomes minimum. A translation of one crystal with respect to the other is called rigid body translation. In the case of a rigid body translation along Y, the shift is related to the volume expansion (or excess volume). Only the relaxed structures with the lowest energy according to the translation in Y have to be considered. Results of this study include the minimum energy for each structure and the shift applied to obtain this minimum.

3.3.3 Energy Minimization Procedure

The minimization procedures may be summarized as follows :

- 1 The perfect lattice is generated for a given crystal structure,
- 2 The list of neighbors of all atoms is created : "the look up list". Only the neighbors in a radius : "the radius of lookup" are considered in the look up list. The interactions with the neighbors beyond this cut-off radius are neglected,
- 3 All the interactions are summed in order to get the unrelaxed energy of the perfect lattice,
- 4 The defect is generated with the starting conditions in 3.3.2 . A new look up list is created and the total energy is computed as the starting energy for the minimization, and

5 the conjugate gradient method is applied to relax the lattice.

3.3.4 General Procedure

The computations were done in Fortran on the Ibm Vax of VPI and SU. An executable file, an input file and the fortran program were needed. The executable file defined the files used inside the main program and gived access to subroutines needed. The parameters in the input files were

- 1 the shifts in X, Y and Z of one crystal with respect to the other, with X and Z axis parallel to the grain boundary plane, Y axis perpendicular to the grain boundary plane, and Z the tilt axis,
- 2 the atom type in a specific site,
- 3 the total number of atoms, and
- 4 the radius of lookup.

For each structure the relationship between the shift in Y and the grain boundary energy was studied in order to find the value of the shift for which the grain boundary energy was minimum. The shift along Y is related to the excess volume. The second parameter allowed us to impose the atom type on the grain boundary plane. The last two parameters are chosen in order to use as less computer time as possible.

The main fortran program was modified to create the appropriate unrelaxed structure. For example, taking an atomic layer out or interchanging atom types in one crystal required to change the program.

In the output file we get the total energy of the perfect crystal, E_{perf} , the total energy of the crystal with the defect (grain boundary), E_{def} , which allowed the calculation of the grain boundary energy, γ_{gb} (see Equation 3.17). The positions of the atoms in the relaxed structure and the displacements of the atoms to get from the positions in the unrelaxed structure to the final positions in the relaxed one are also presented in the output file.

4 RESULTS

The boundaries considered in this study are $[001]$ symmetrical tilt boundaries with low reciprocal coincident site density Σ in NiAl B2 phase : $\Sigma = 5(210)$, $\Sigma = 5(310)$, $\Sigma = 29(520)$, and some aspects of the $[1\bar{1}0]$ symmetrical tilt boundary : $\Sigma = 3(11\bar{2})$. Both the $\Sigma = 5(210)$ and the $\Sigma = 5(310)[001]$ tilt boundaries are favored according to the CSL and structural unit model summarized in section 2.2 . As explained in section 2.2 favored boundaries are short period boundaries and are usually associated with low grain boundary energy. The periods of the favored boundaries are found to be fundamental units of longer period boundaries. In addition, features of the favored boundaries such as the atomic structure or the stress field may be used to predict features in the non-favored ones. Thus, we will put particular emphasis on both favored boundaries mentioned above. All the grain boundary

structures presented in this study are shown in a projection of atoms on a plane perpendicular to the tilt axis. For $[001]$ tilt boundaries the plane is (001) , and for $[1\bar{1}0]$ tilt boundaries it is $(1\bar{1}0)$. Such a representation brings the grain boundary plane perpendicular to the paper. In all pictures the boundary plane is represented horizontal. Filled circles and triangles correspond to nickel and open ones to aluminum. Due to the representation of the boundaries in the projection on the (001) (or $(1\bar{1}0)$) plane only two atomic planes parallel to the paper need to be considered. The triangles and circles represent atoms in these two different (001) (or $(1\bar{1}0)$) planes.

4.1 $[001]$ Symmetrical Tilt Boundaries

4.1.1 $\Sigma = 5(210)$ *Symmetrical Tilt Boundary*

In this section, all the changes described in section 3.3.2 are applied on the unrelaxed grain boundary, in order to obtain all the possible relaxed structures. As a result of the changes, such as removing layers or interchanging the atom types (changing all nickel for aluminum and aluminum for nickel) in one crystal, different grain boundary stoichiometries can be obtained. We emphasize stoichiometric boundaries and also boundaries that are one atom rich (Al or Ni) boundaries per structural unit. The structural unit is defined as the three dimensional repeat cell which is the period of the boundary (see section 3.2). Throughout all this work the stoichiometry of the boundaries will be referred by the number of excess atoms per structural unit. We are interested in observing trends on the atomic structures and the energies of the

boundaries. The energy values calculated by computer simulation should always be taken as semiquantitative, and used to study trends. Two atoms rich (Al or Ni) boundaries in Figures 33, 34 and 35 will confirm all the considered trends.

4.1.1.1 Stoichiometric $\Sigma = 5(210)$ Grain Boundary Structures (Figures (4-14))

The possible relaxed structures for stoichiometric configurations are represented in Figures 4 to 14. The structures in Figures 4 and 5 are the basic structures obtained by misorientation of the two crystals according to the CSL. These two structures are identical except that the boundary content is nickel for the structure in Figure 4 and aluminum in Figure 5. They are the starting point of the modifications which can be made (see part 3.3.2) in order to get all possible structures. Figures 6 and 7 are simply obtained from Figures 4 and 5 by translating one crystal with respect to the other by $\frac{1}{2}\alpha_0$ along the Z direction (Z is the tilt axis (001) as explained in section 3.3.1). From these results we see that structures with nickel atoms on the boundary (Figures 4 and 6) give higher grain boundary energy. We obtain the structures in Figures 8 and 9 by applying the shift of $\frac{1}{2}\alpha_0$ along the Z direction on the atoms in the grain boundary plane of the unrelaxed structure. Only atoms located on the grain boundary are shifted from their original (001) plane to a parallel one. This leads to high energy structures. Structures 10 to 13 are the structures resulting from removing an atomic layer plus making the $\frac{1}{2}\alpha_0$ shift in Z or interchanging atom types. The structure in Figure 14 is the same as in Figures 10 or 11 except that atoms on the boundary plane lay in the same (001) plane. This structure has a high grain boundary energy value.

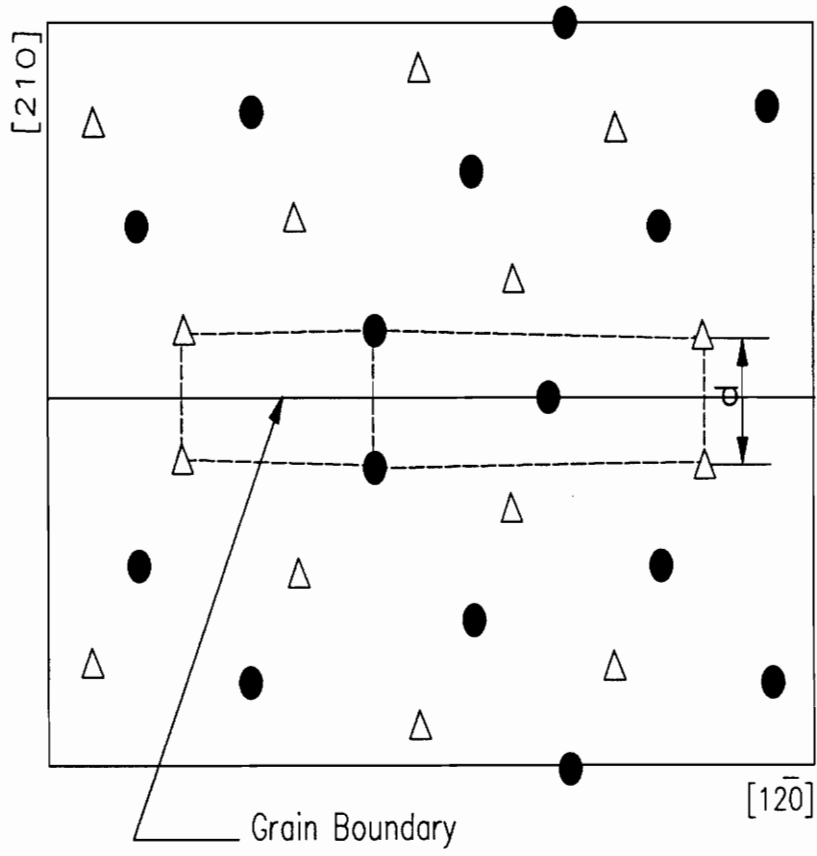


Figure 4. Stoichiometric $\Sigma = 5(210)$ grain boundary structure
 $+0.96 \text{ \AA}$ shift, $1,448 \text{ mJ/m}^2$ grain boundary energy

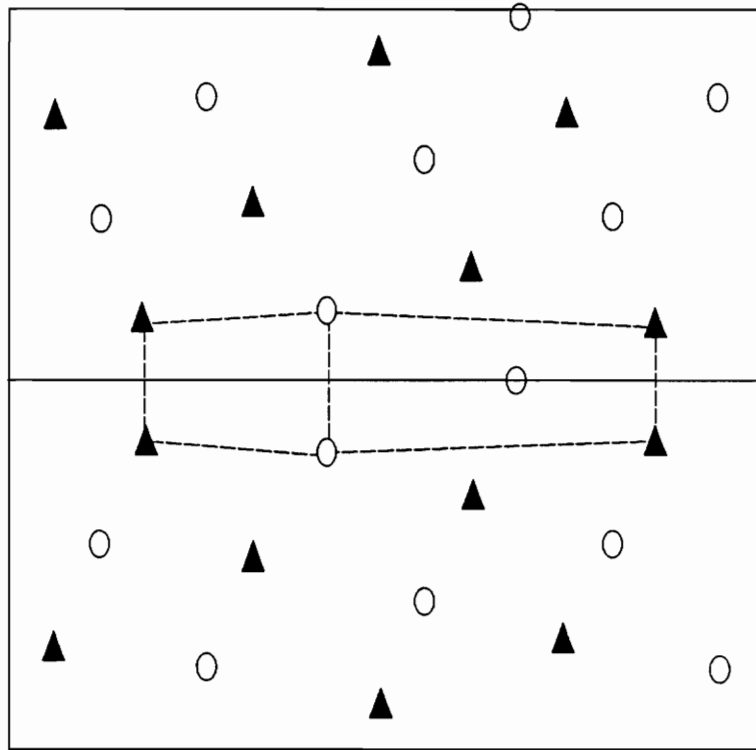


Figure 5. Stoichiometric $\Sigma = 5(210)$ grain boundary structure
+0.88 Å shift, 892 mJ/m² grain boundary energy

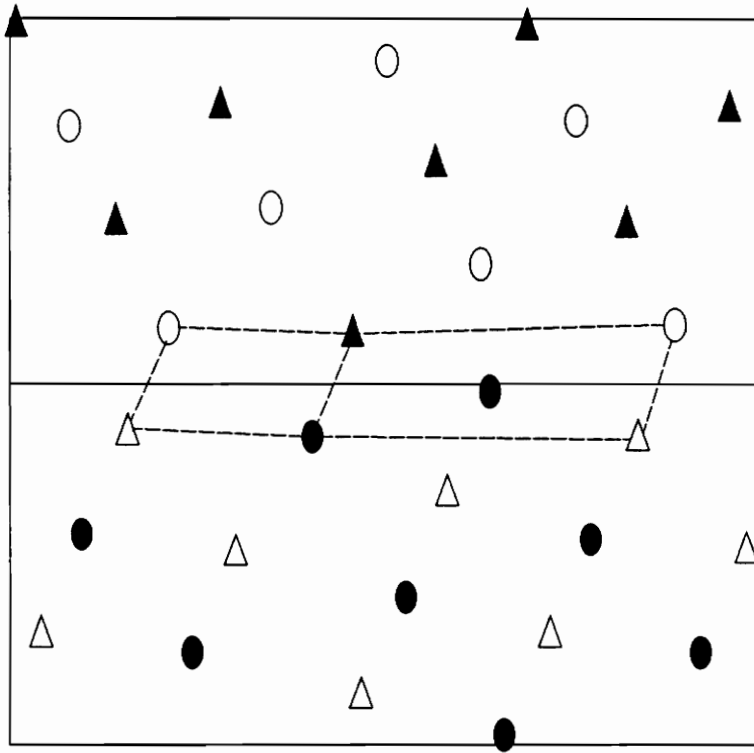


Figure 6. Stoichiometric $\Sigma = 5(210)$ grain boundary structure
+0.73 Å shift, 963 mJ/m² grain boundary energy

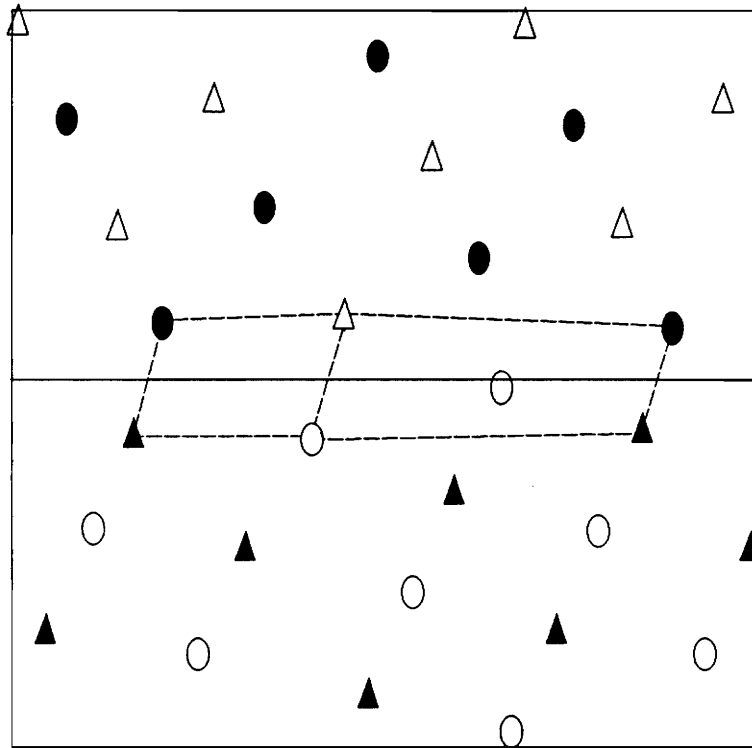
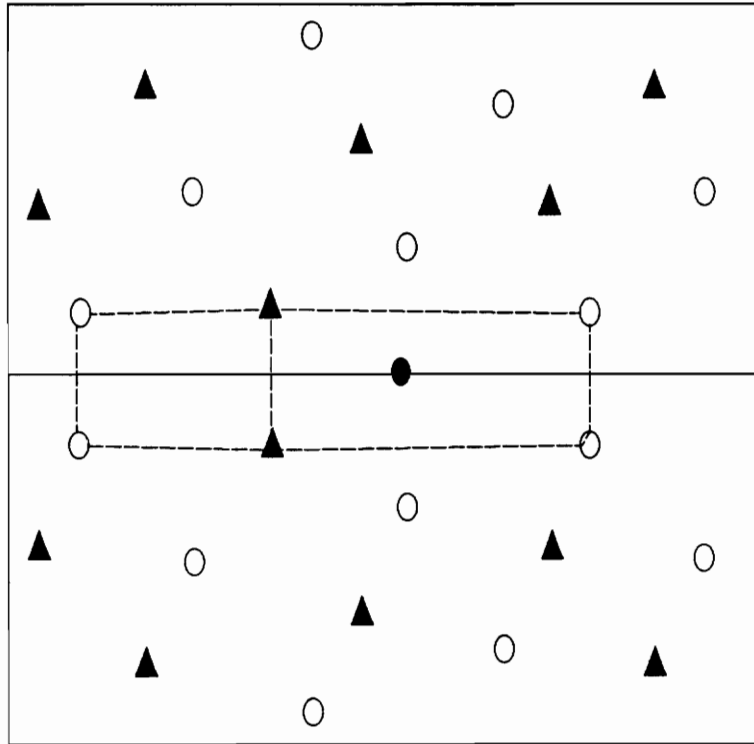


Figure 7. Stoichiometric $\Sigma = 5(210)$ grain boundary structure
+0.64 Å shift, 767 mJ/m² grain boundary energy



**Figure 8. Stoichiometric $\Sigma = 5(210)$ grain boundary structure
+1.20 Å shift, 1,713 mJ/m² grain boundary energy**

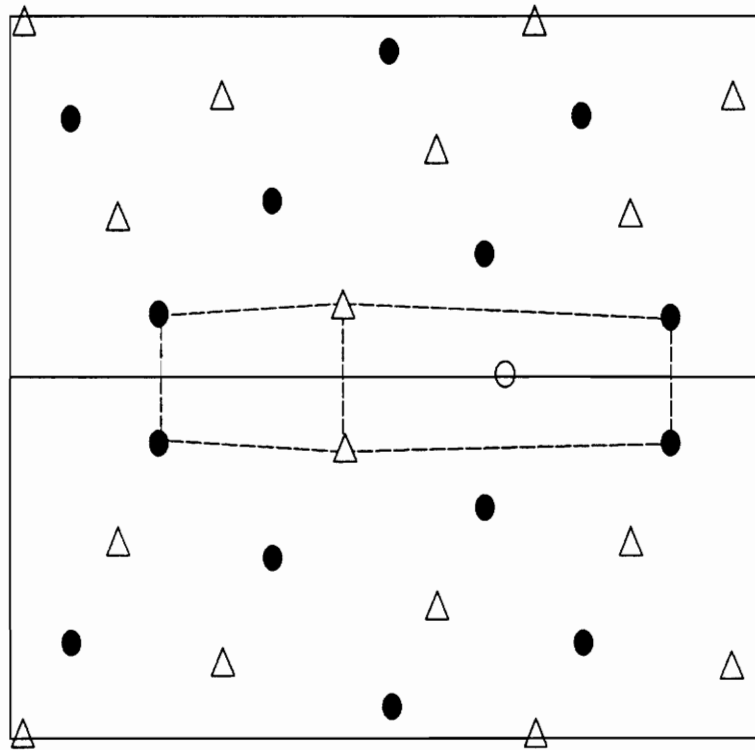


Figure 9. Stoichiometric $\Sigma = 5(210)$ grain boundary structure
 +1.09 Å shift, 1,483 mJ/m² grain boundary energy

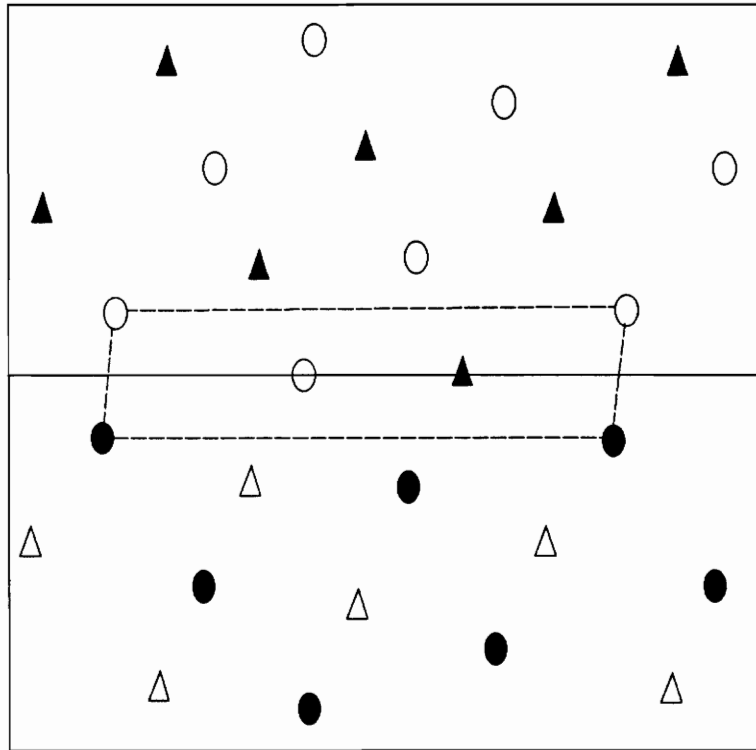


Figure 10. Stoichiometric $\Sigma = 5(210)$ grain boundary structure
 $+0.06 \text{ \AA}$ shift, 910 mJ/m^2 grain boundary energy

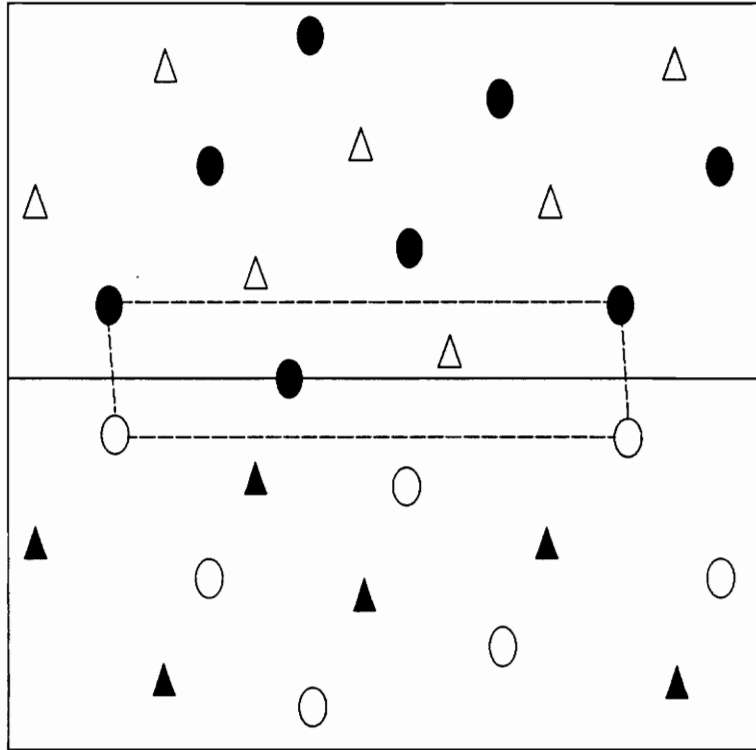


Figure 11. Stoichiometric $\Sigma = 5(210)$ grain boundary structure
+0.03 Å shift, 746 mJ/m² grain boundary energy

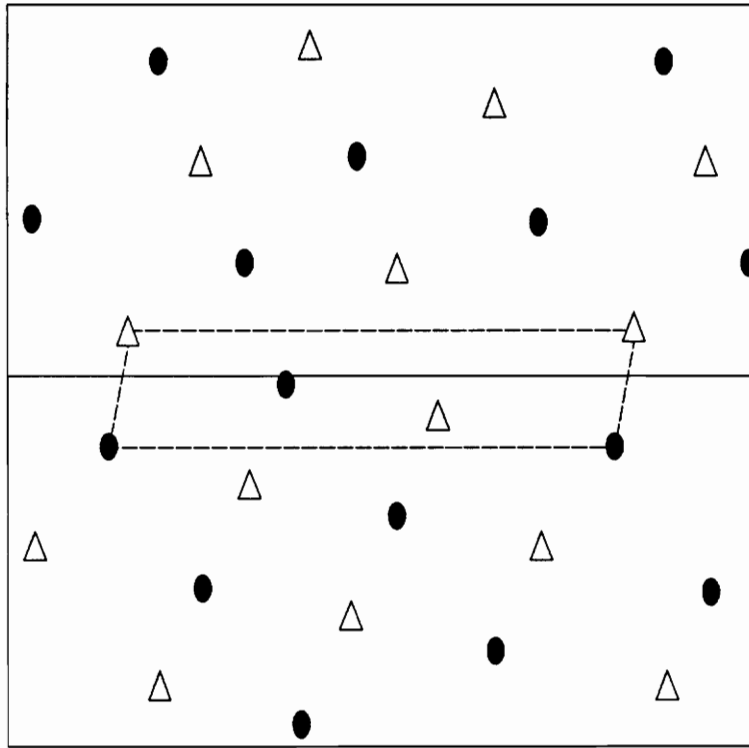


Figure 12. Stoichiometric $\Sigma = 5(210)$ grain boundary structure
 $+0.33 \text{ \AA}$ shift, 899 mJ/m^2 grain boundary energy

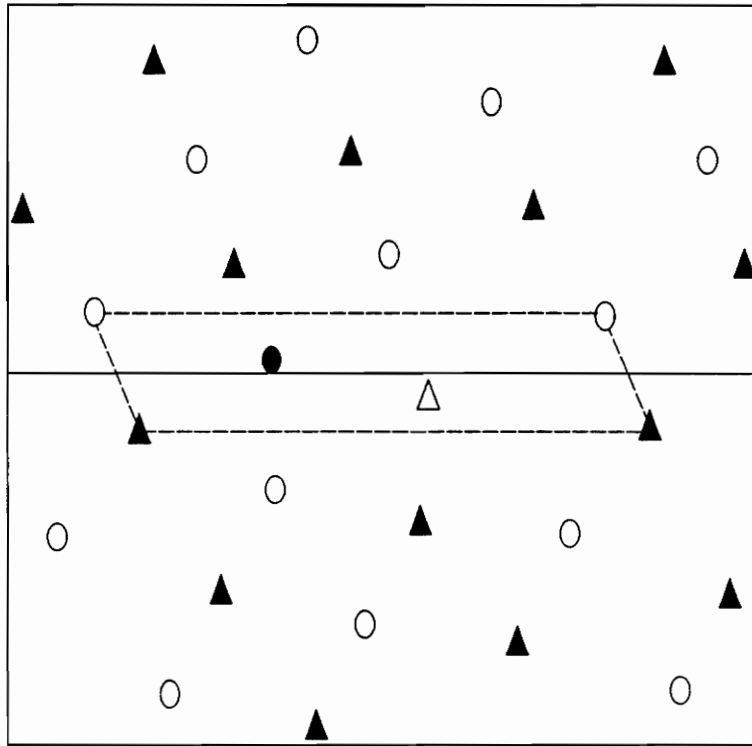


Figure 13. Stoichiometric $\Sigma = 5(210)$ grain boundary structure
+0.28 Å shift, 1,221 mJ/m² grain boundary energy

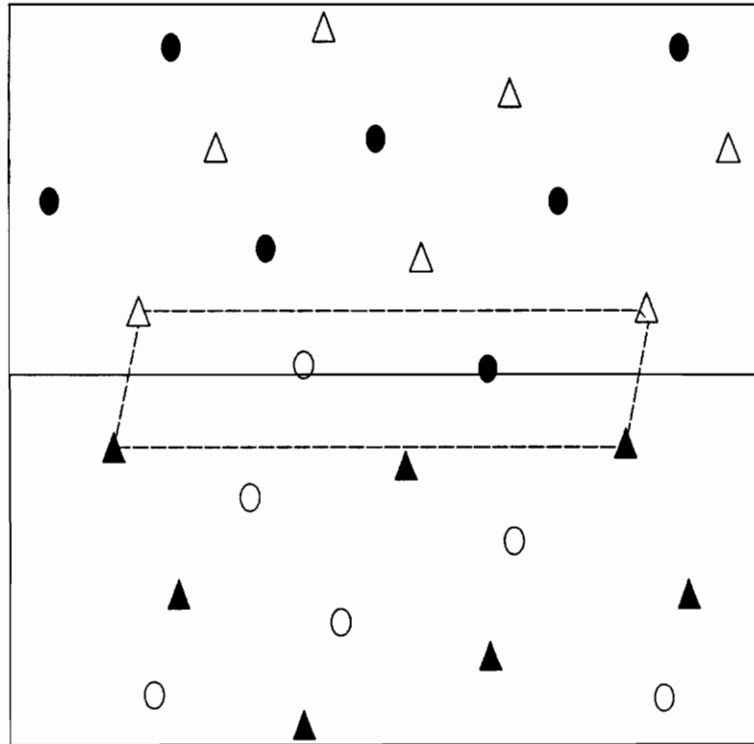


Figure 14. Stoichiometric $\Sigma = 5(210)$ grain boundary structure
+0.53 Å shift, 1,661 mJ/m² grain boundary energy

4.1.1.2 One atom rich $\Sigma = 5(210)$ Grain Boundary Structures (Figures (15-32))

Figures 15 to 23 show structures with one excess nickel atom per structural unit. The structure in Figure 16 results from interchanging atom types in one of the crystals in the structure of Figure 4. Figure 15 is then obtained from Figure 16 by applying the $\frac{1}{2}\alpha_0$ shift along Z to one crystal with respect to the other. Using the exact same shift as used previously on atoms located on the boundary plane of the unrelaxed structure of Figure 16, yields the structure of Figure 17. For Figures 18 to 21 an atomic layer of aluminum atoms is taken out, and, for Figures 22 and 23 the atomic layer removed is one of nickel atoms. Indeed, the structure in Figure 18 is similar to the one in Figure 4 with an aluminum content layer removed. Then, the relaxed structure in Figure 18 exhibits two atoms per period on the boundary. The $\frac{1}{2}\alpha_0$ shift along Z is applied on these two atoms in order to obtain the structure in Figure 19. Figures 20 and 21 come from Figure 18 with a translation of $\frac{1}{2}\alpha_0$ in Z of one crystal with respect to the other. Positions of the atoms on the grain boundary of the relaxed structures make the difference between structures in Figure 20 and 21. Structure of Figure 21 has the atoms on the boundary plane laying in the same (001) plane. This structure exhibits a relatively high energy compared to the other one excess nickel atom structures. In general one nickel atom rich structures have lower grain boundary energies than stoichiometric structures.

Structures in Figures 24 to 32 present the one excess aluminum atom grain boundary structures. These structures are completely equivalent to the Ni rich structures seen previously. The atom types were interchanged within both crystals yielding to one excess aluminum instead of one excess nickel. This time, energies appear to be higher than in the stoichiometric structure case, and even much higher than for the one nickel rich structures. When we compare energies of a one nickel rich structures and the equivalent one aluminum rich with atom types interchanged (Figures 15 and 24 for example, or 16 and 25...), the nickel rich structure is always the low energy one.

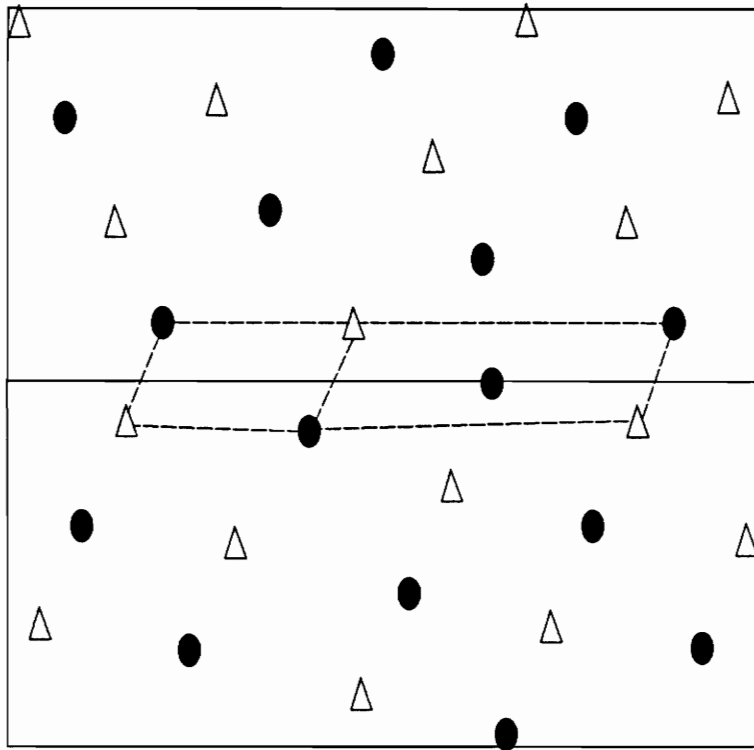


Figure 15. One excess Ni atom $\Sigma = 5(210)$ grain boundary structure
+0.61 Å shift, 427 mJ/m² grain boundary energy

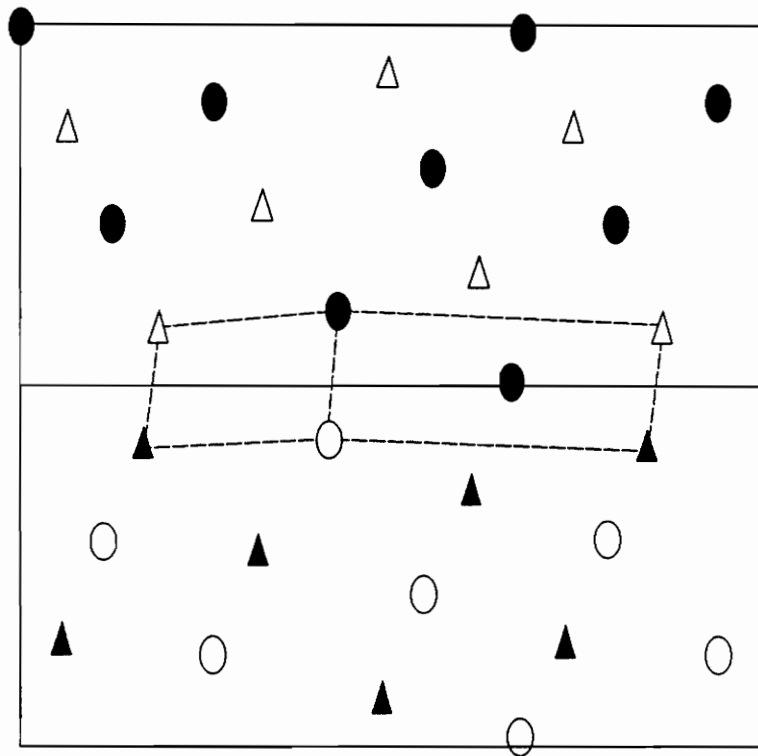


Figure 16. One excess Ni atom $\Sigma = 5(210)$ grain boundary structure
 +0.82 Å shift, 895 mJ/m² grain boundary energy

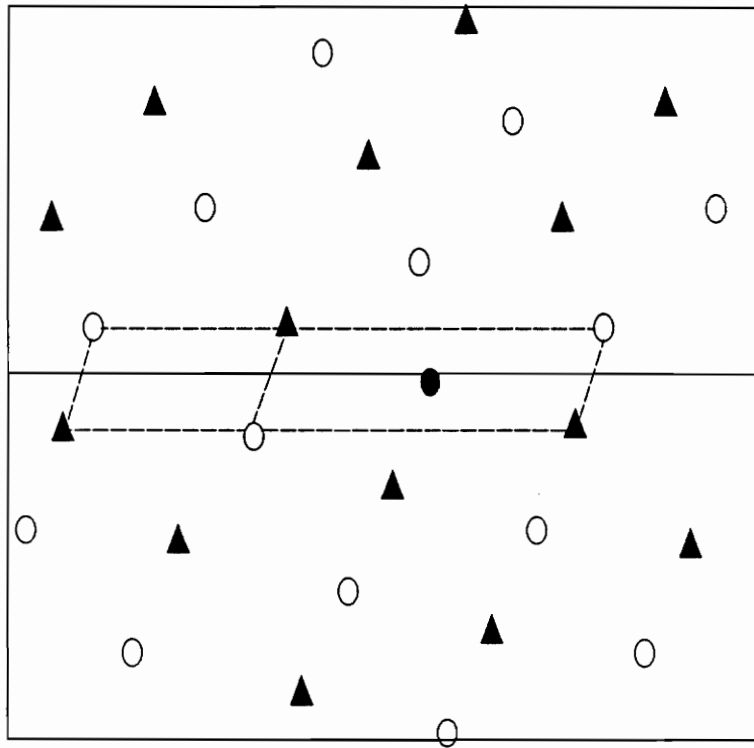


Figure 17. One excess Ni atom $\Sigma = 5(210)$ grain boundary structure
 +0.73 Å shift, 540 mJ/m² grain boundary energy

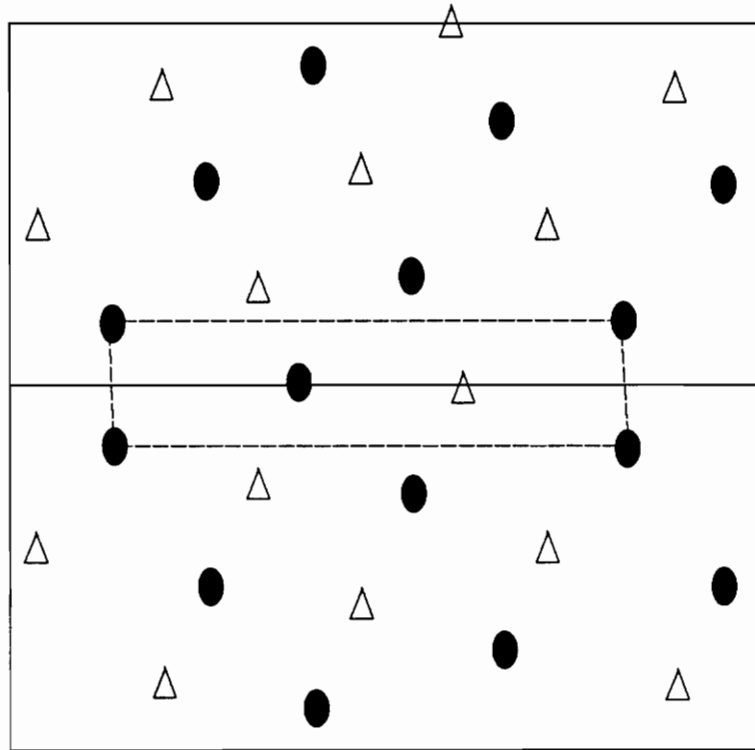


Figure 18. One excess Ni atom $\Sigma = 5(210)$ grain boundary structure
-0.11 Å shift, 386 mJ/m² grain boundary energy

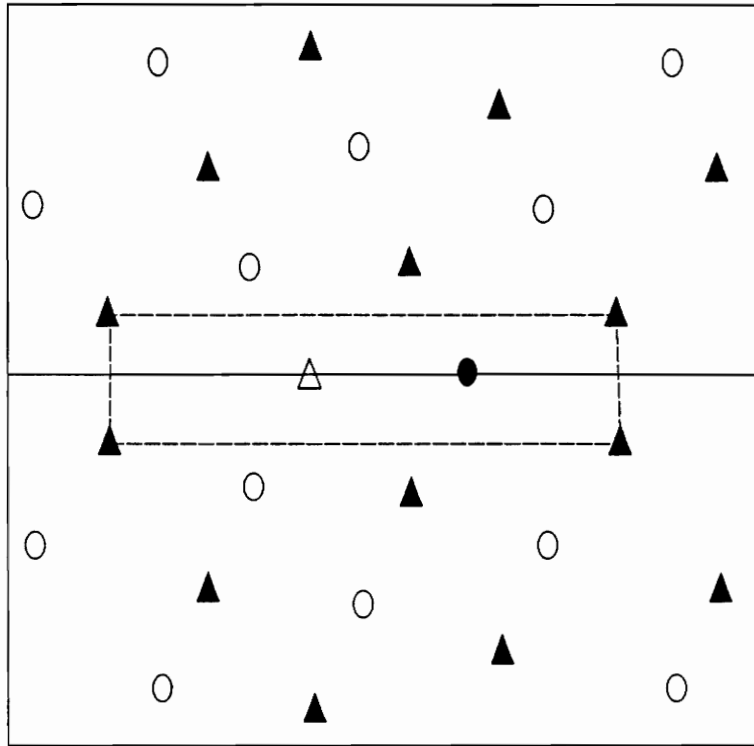


Figure 19. One excess Ni atom $\Sigma = 5(210)$ grain boundary structure
+0.10 Å shift, 971 mJ/m² grain boundary energy

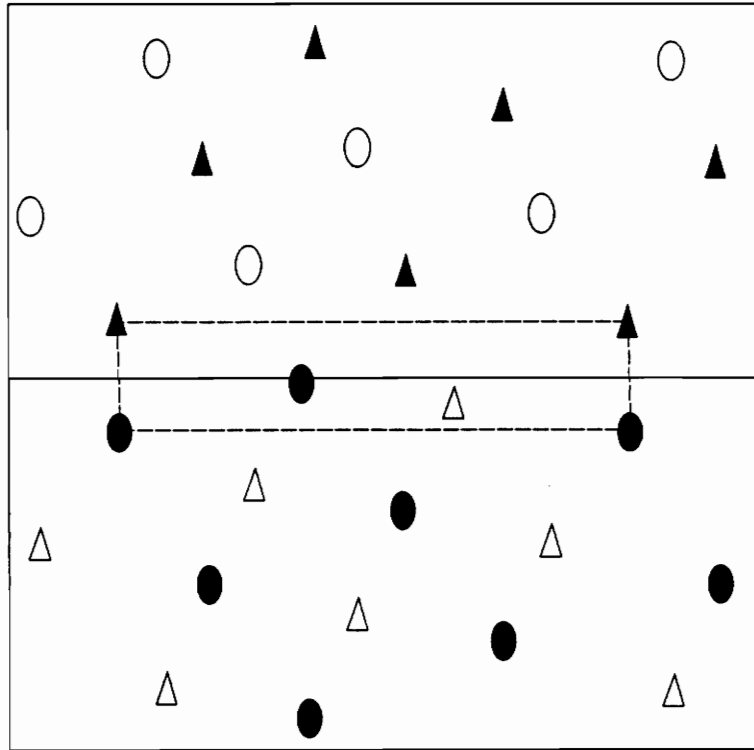


Figure 20. One excess Ni atom $\Sigma = 5(210)$ grain boundary structure
+0.09 Å shift, 936 mJ/m² grain boundary energy

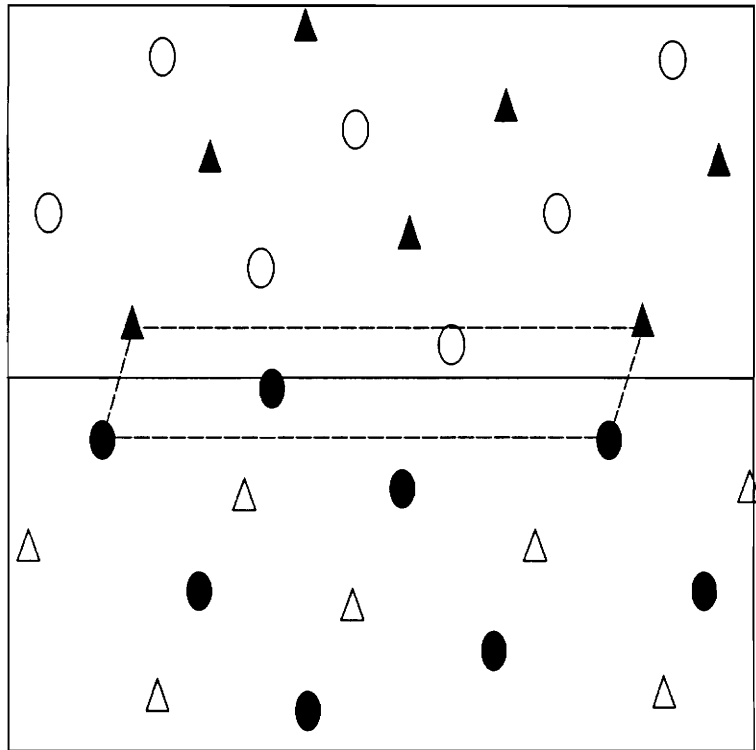


Figure 21. One excess Ni atom $\Sigma = 5(210)$ grain boundary structure
+0.25 Å shift, 1,108 mJ/m² grain boundary energy

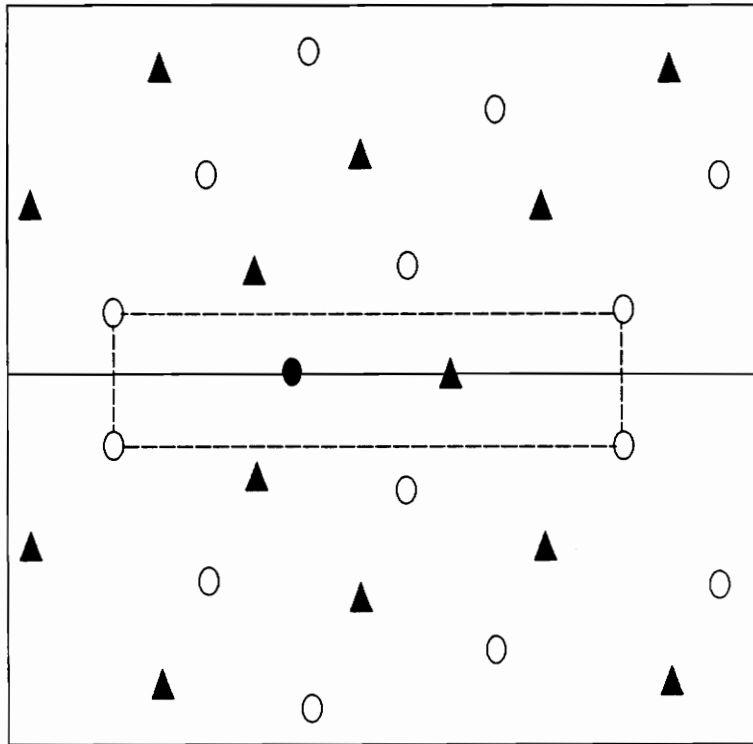


Figure 22. One excess Ni atom $\Sigma = 5(210)$ grain boundary structure
+0.11 Å shift, 599 mJ/m² grain boundary energy

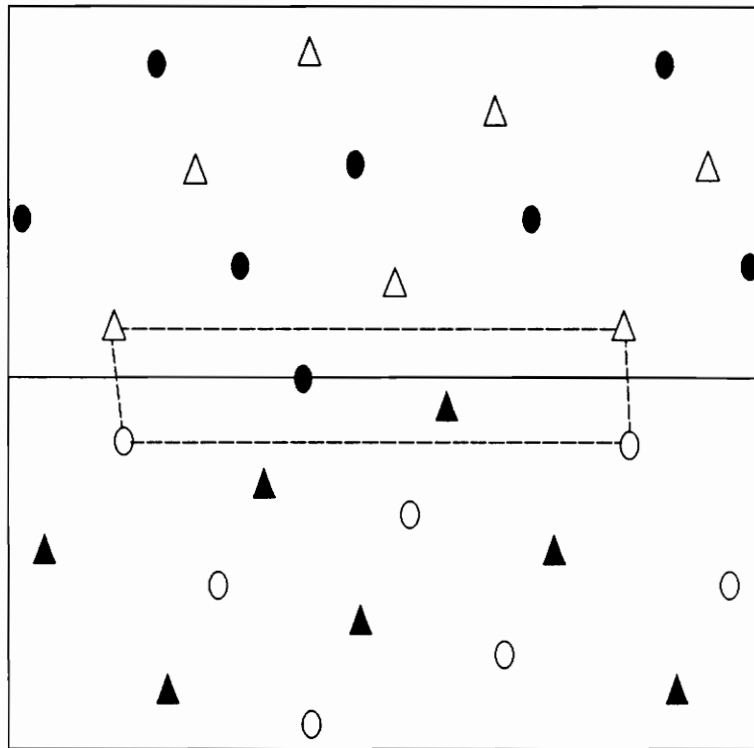


Figure 23. One excess Ni atom $\Sigma = 5(210)$ grain boundary structure
 +0.21 Å shift, 786 mJ/m² grain boundary energy

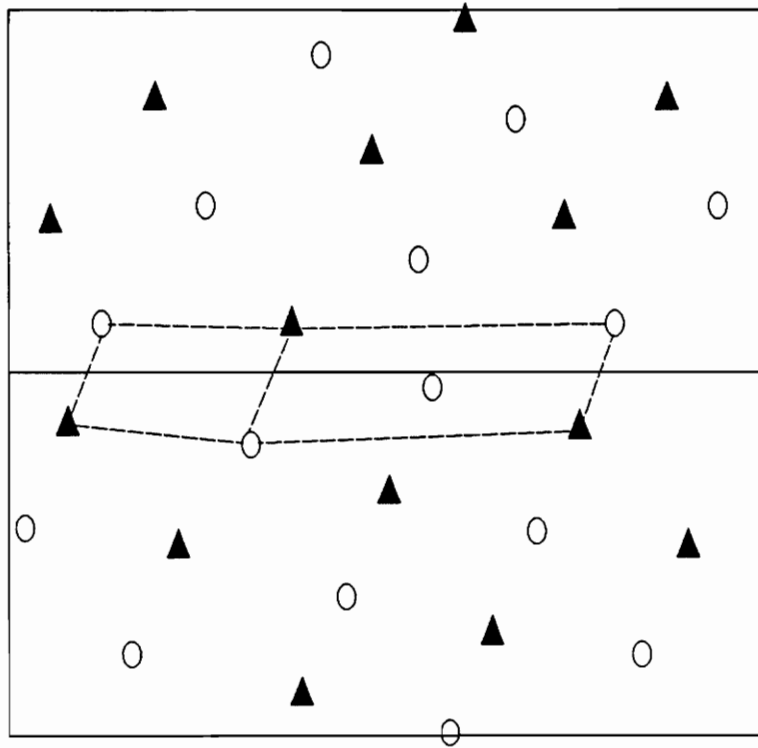


Figure 24. One excess Al atom $\Sigma = 5(210)$ grain boundary structure
+0.88 Å shift, 1,140 mJ/m² grain boundary energy

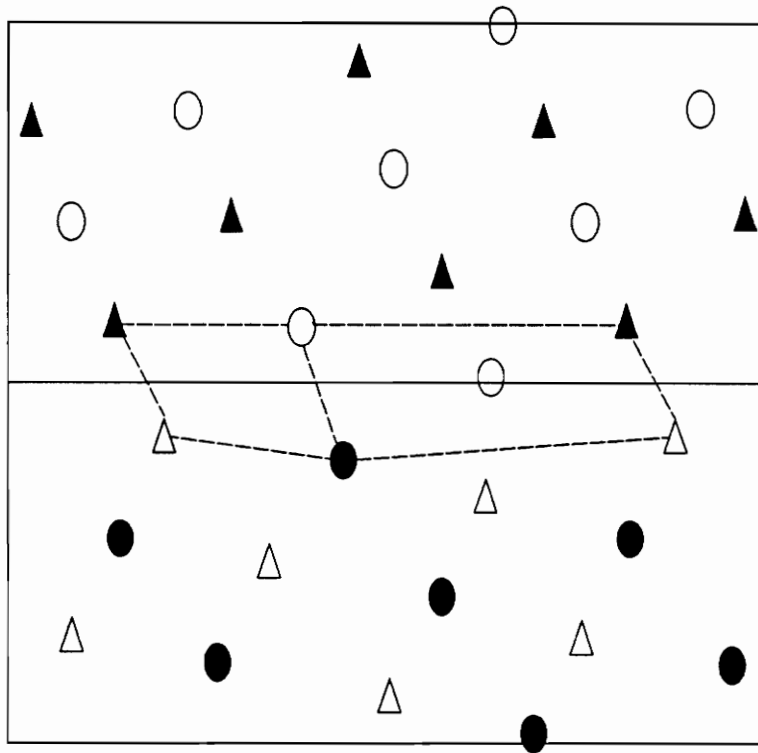


Figure 25. One excess Al atom $\Sigma = 5(210)$ grain boundary structure
 +0.96 Å shift, 1,350 mJ/m² grain boundary energy

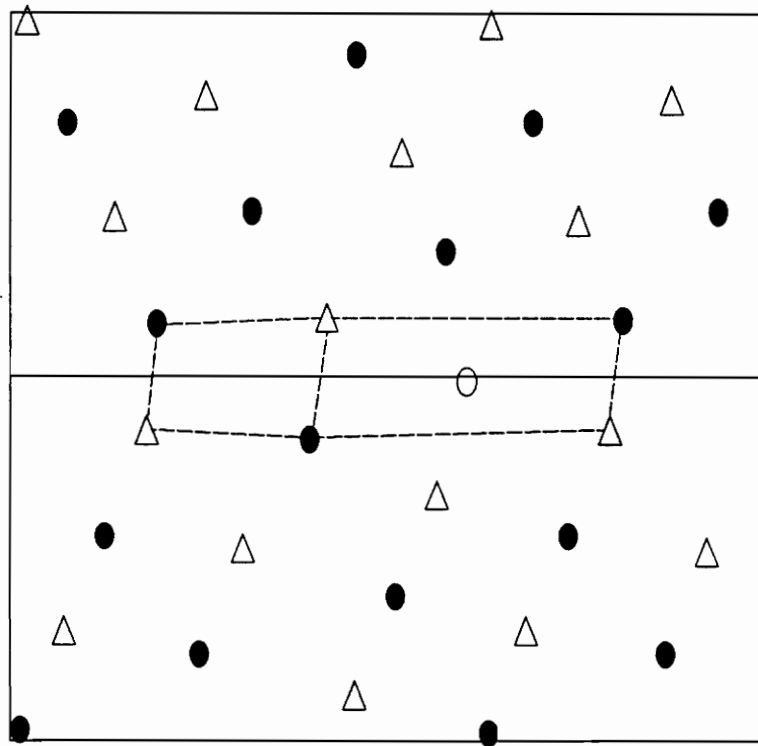


Figure 26. One excess Al atom $\Sigma = 5(210)$ grain boundary structure
 +0.72 Å shift, 1,337 mJ/m² grain boundary energy

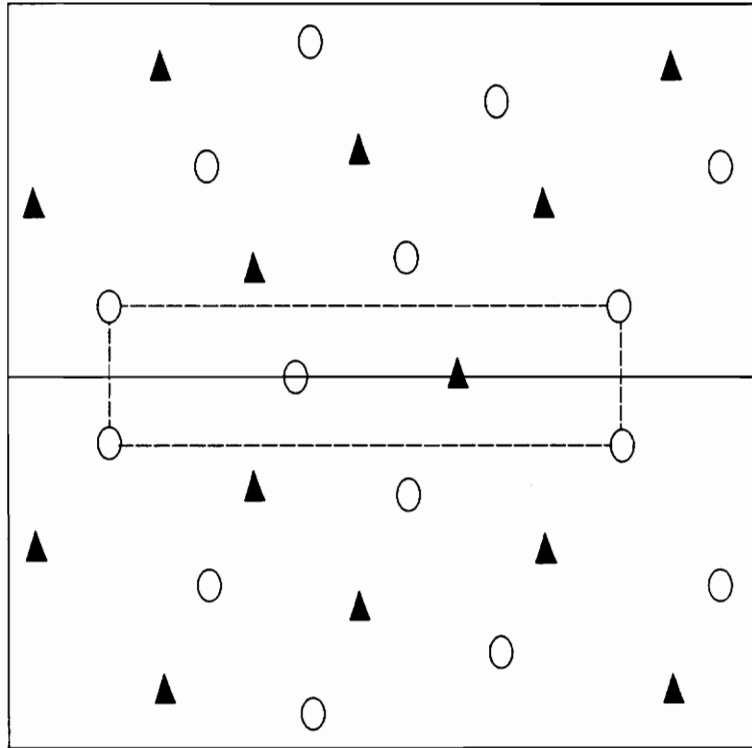


Figure 27. One excess Al atom $\Sigma = 5(210)$ grain boundary structure
+0.08 Å shift, 1,108 mJ/m² grain boundary energy

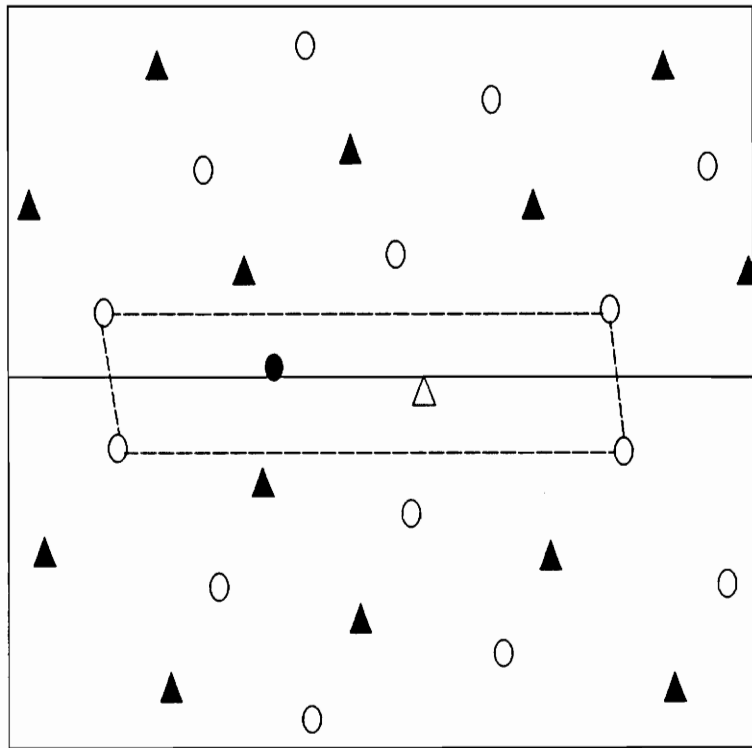


Figure 28. One excess Al atom $\Sigma = 5(210)$ grain boundary structure
+0.18 Å shift, 1,357 mJ/m² grain boundary energy

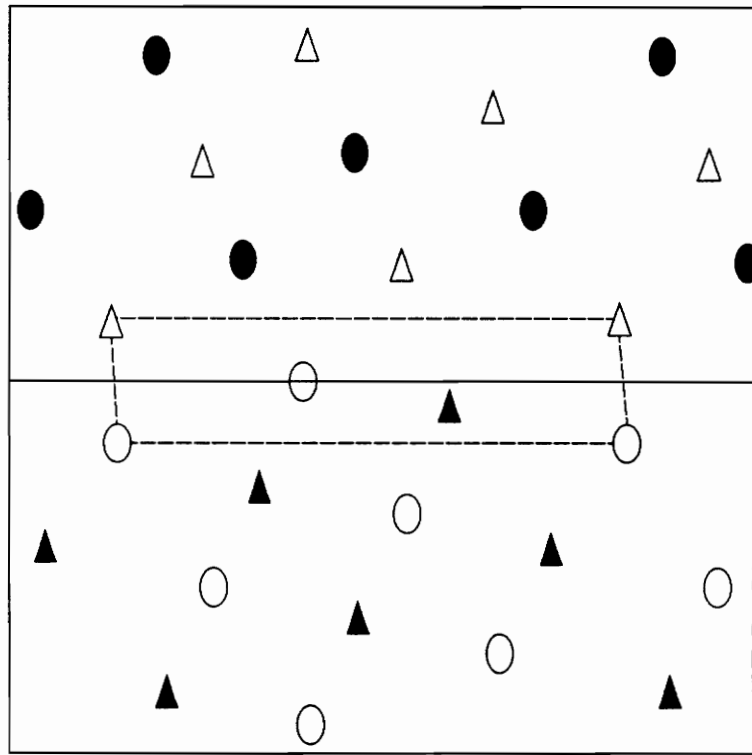


Figure 29. One excess Al atom $\Sigma = 5(210)$ grain boundary structure
+0.14 Å shift, 1,308 mJ/m² grain boundary energy

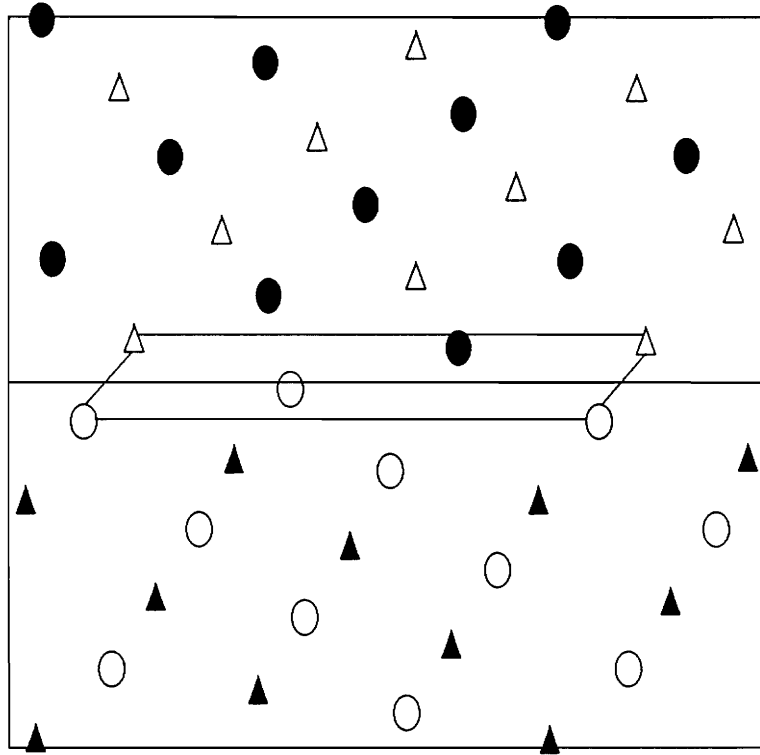


Figure 30. One excess Al atom $\Sigma = 5(210)$ grain boundary structure
+0.51 Å shift, 1,607 mJ/m² grain boundary energy

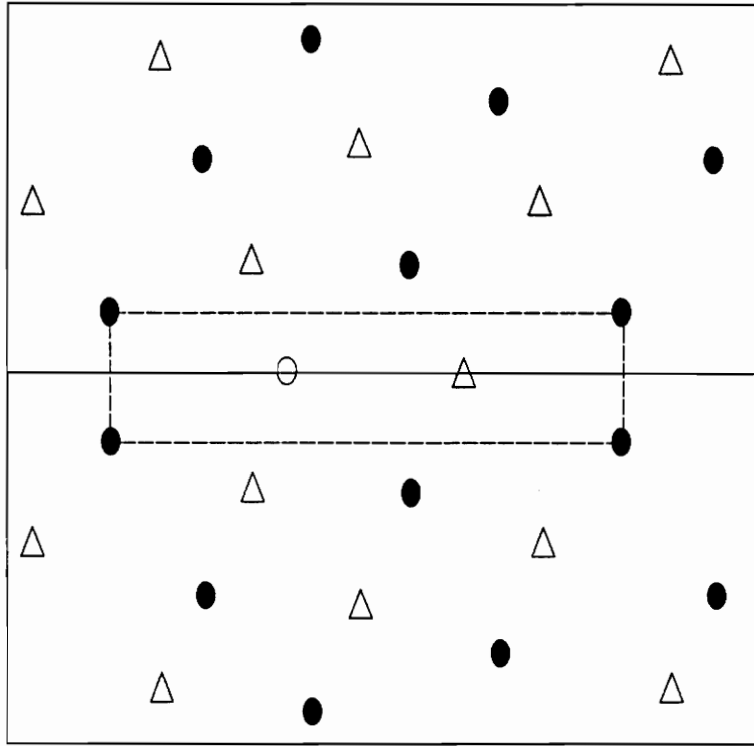


Figure 31. One excess Al atom $\Sigma = 5(210)$ grain boundary structure
+0.28 Å shift, 1,441 mJ/m² grain boundary energy

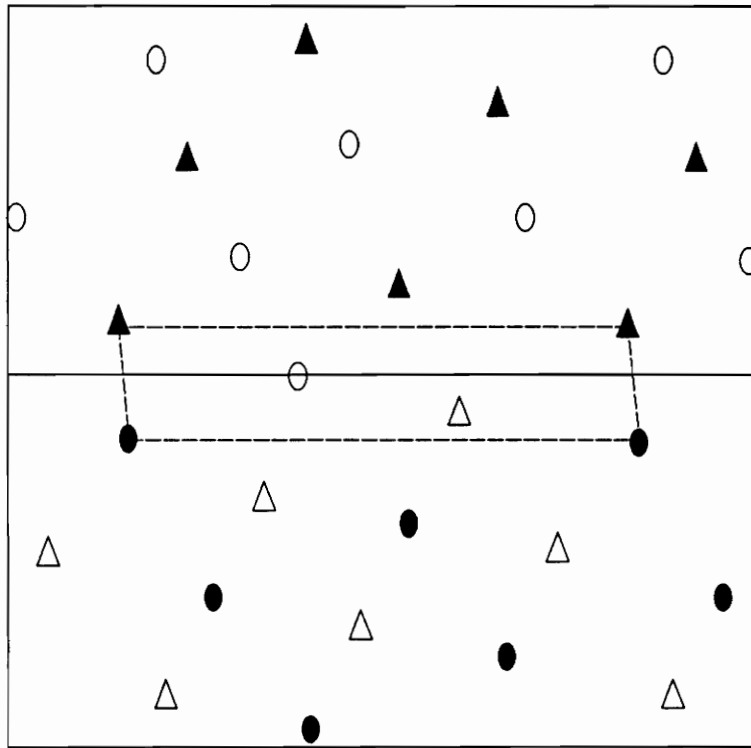


Figure 32. One excess Al atom $\Sigma = 5(210)$ grain boundary structure
 +0.41 Å shift, 1,940 mJ/m² grain boundary energy

4.1.1.3 Two atoms rich $\Sigma = 5(210)$ Grain Boundary Structures (Figures (33-35))

Both Figures 33 and 34 were obtained by interchanging atom types in one crystal and removing an atomic layer. In Figure 33 the removed atomic layer is aluminum and in Figure 34 it is nickel. Figure 35 is the same as 33 except that Ni atoms on the grain boundary are in the same (001) plane. A similar configuration was not considered for the two Al rich structure according to the already relatively high grain boundary energy obtained for the two Ni rich one. Indeed, the absolute value of the energy of the two Ni atoms rich structure is not high, but it should be much lower according to the trend discussed in section 5 (see also Figure 36). The two excess nickel atoms structure (Figure 33) has a very low energy and the two excess aluminum atoms structure (Figure 34) has a very high one.

We note that having two atoms at the interface plane on the same (001) plane has always lead to high energy structures. The structure of Figure 35 (Ni atoms rich structure), but also the stoichiometric one of Figure 14, the one Ni atom rich of Figure 21, and also the one Al atom rich structure of Figure 30 yield relatively high grain boundary energies. We conclude that configurations in which atoms at the interface lay on the same (001) plane will always tend to have high energies and therefore need not be considered.

Finally, for $\Sigma = 5(210)$ boundary the results can be represented by plotting the grain boundary energy as a function of the stoichiometry (Figure (36)). This plot exhibits the trend that the grain boundary energy depends on the stoichiometry. As the excess in aluminum gets higher, the energy increases.

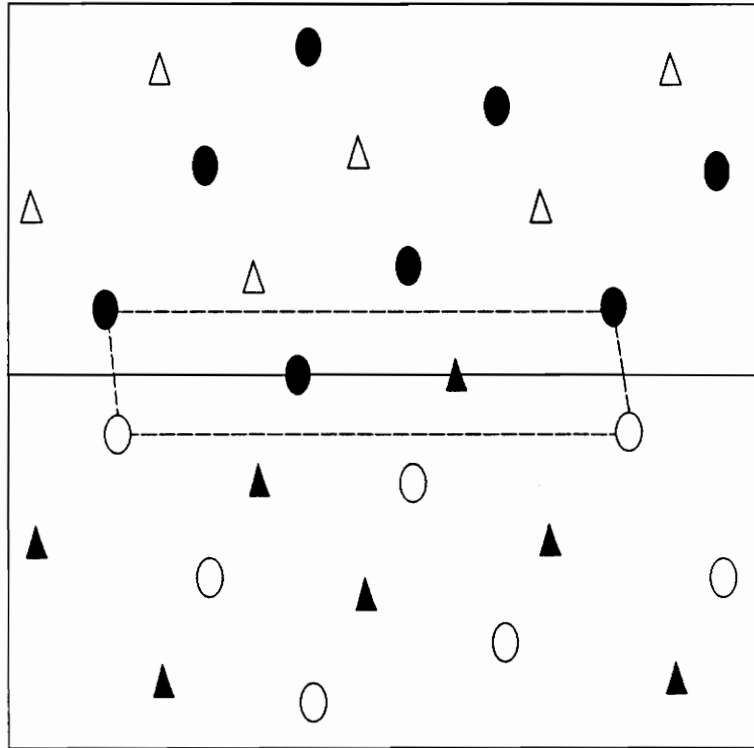


Figure 33. Two excess Ni atoms $\Sigma = 5(210)$ grain boundary structure
 -0.03 \AA shift, 342 mJ/m^2 grain boundary energy

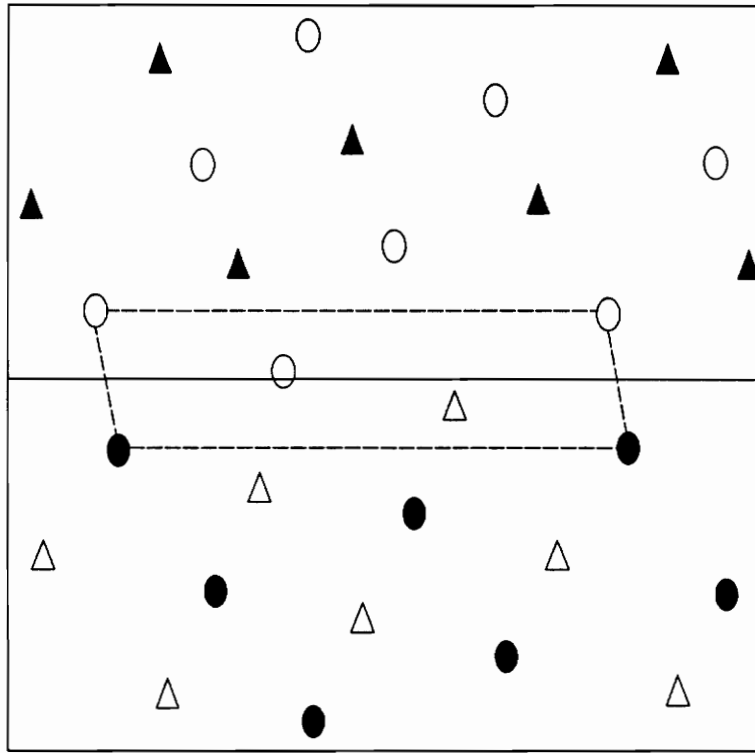


Figure 34. Two excess Al atoms $\Sigma = 5(210)$ grain boundary structure
 +0.30 Å shift, 1,739 mJ/m² grain boundary energy

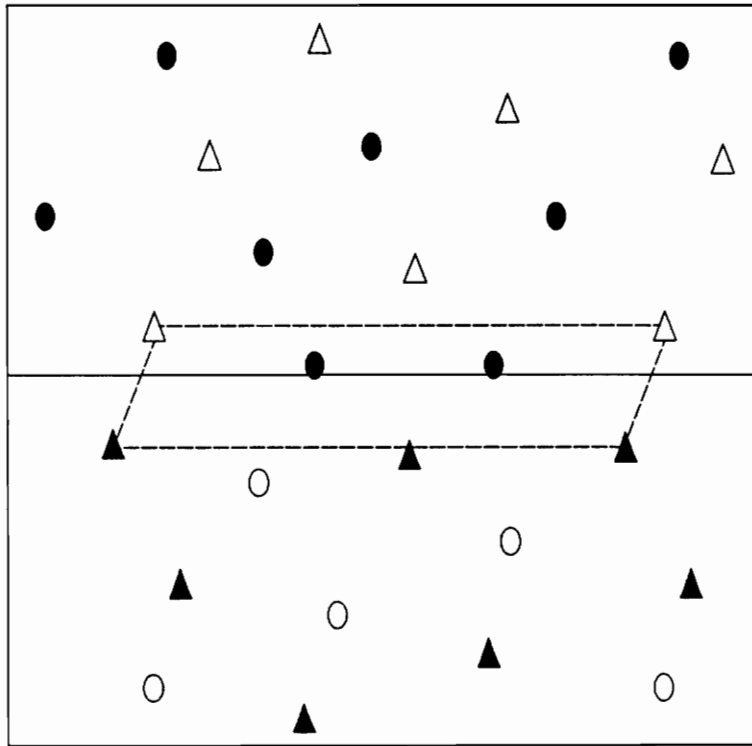
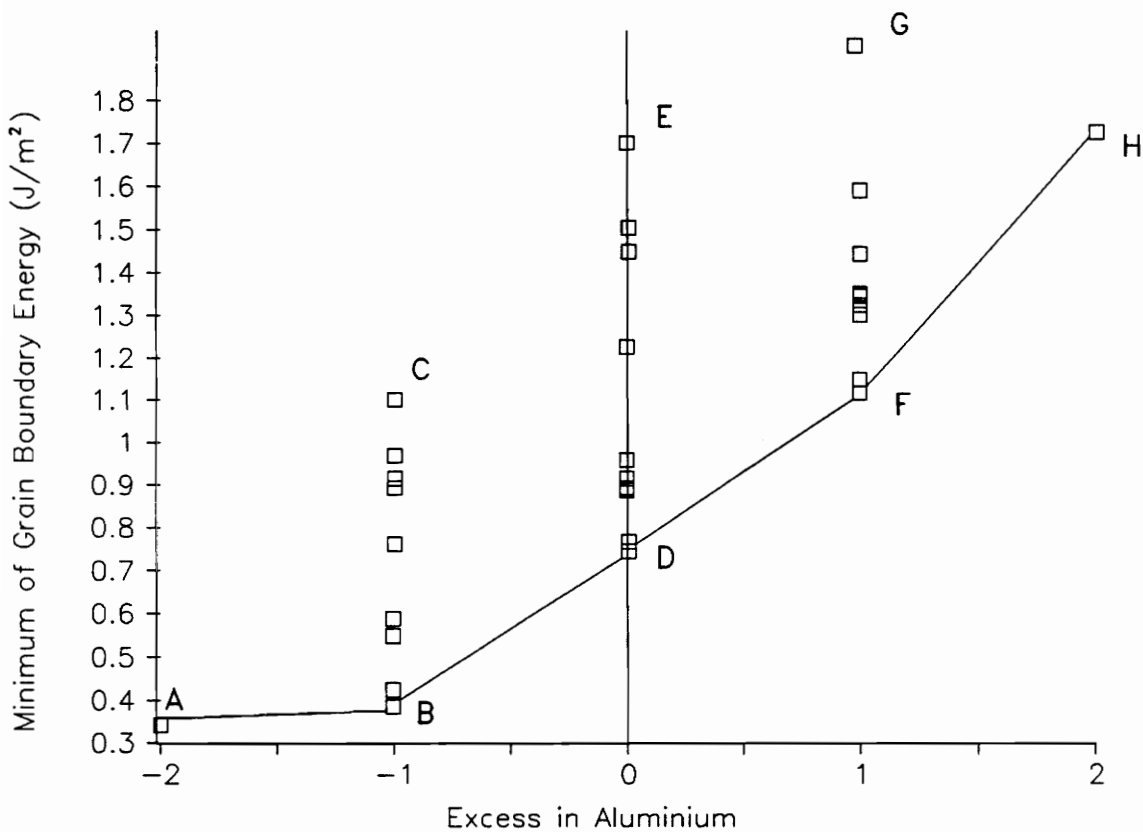


Figure 35. Two excess Ni atoms $\Sigma = 5(210)$ grain boundary structure
 +0.12 Å shift, 1,137 mJ/m² grain boundary energy



Point A : Figure 33

Point B to C : Figures 15 to 23

Point D to E : Figures 4 to 14

Point F to G : Figures 24 to 32

Point H : Figure 35

Figure 36. Grain boundary energy as a function of excess in aluminum for $\Sigma = 5(210)$ grain boundary structures

4.1.2 $\Sigma = 5(310)$ *Symmetrical Tilt Boundary*

For this plane only the stoichiometric boundaries are considered (Figures 37 to 45). The parallel planes to the grain boundary for the unrelaxed structure are always of equiatomic composition 50% Ni and 50% Al. So, removing layers, or interchanging atom types does not change the stoichiometry. In addition, the boundary content has also 50% Al and 50% Ni composition. The distinction between nickel or aluminum boundary content made for the boundary $\Sigma = 5(210)$ is not applied in this case. This particularity brings about less possible configurations than in the $\Sigma = 5(210)$ case.

The basic structure is pictured in Figure 38. Interchanging atom types in one crystal gives the structure of Figure 39. Then, applying the $\frac{1}{2}\alpha_0$ shift along Z to one of the crystal of the structure in Figure 39 results in the structure in Figure 37. The structure in Figure 40 is obtained by applying the same shift in Z to one crystal in the structure of Figure 38. Figures 41 to 43 were constructed by removing an atomic layer parallel to the boundary plane. Removing an atomic layer yields relatively high energy structures.

4.1.3 $\Sigma = 29(520)$ *Symmetrical Tilt Boundary*

The creation of the $\Sigma = 29(520)$ boundary by the simple mirror operation (see section 3.3.2) appears to give very high energy structures (Figures 46 and 47) with big holes, even with one atomic layer taken out (Figures 48 and 49). It seems that a nickel atom is missing on the boundary plane for Figures 46 and 48, and an aluminum atom in Figures 47 and 49.

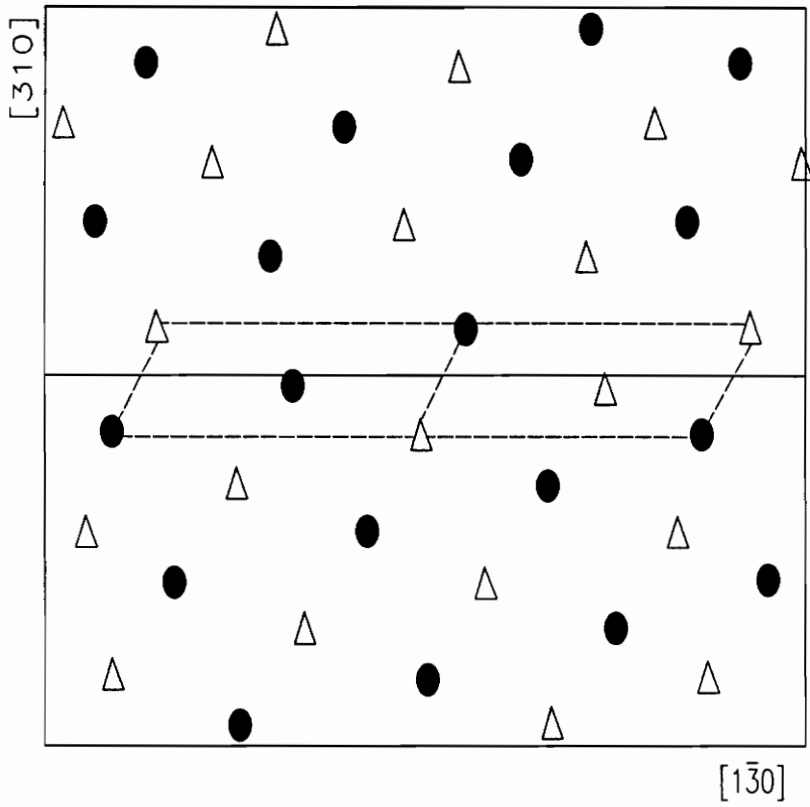


Figure 37. Stoichiometric $\Sigma = 5(310)$ grain boundary structure
 +0.73 Å shift, 855 mJ/m² grain boundary energy

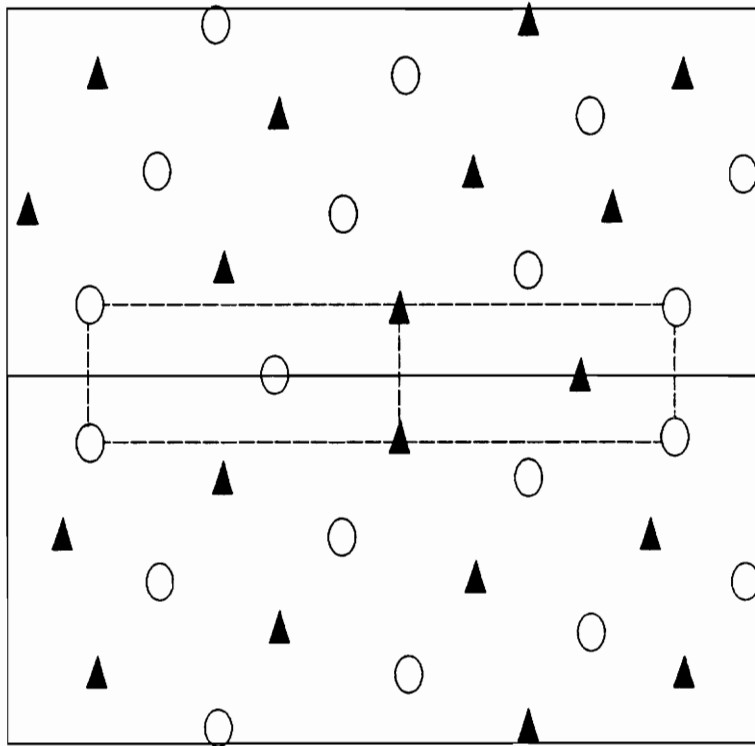


Figure 38. Stoichiometric $\Sigma = 5(310)$ grain boundary structure
 +0.65 Å shift, 825 mJ/m² grain boundary energy

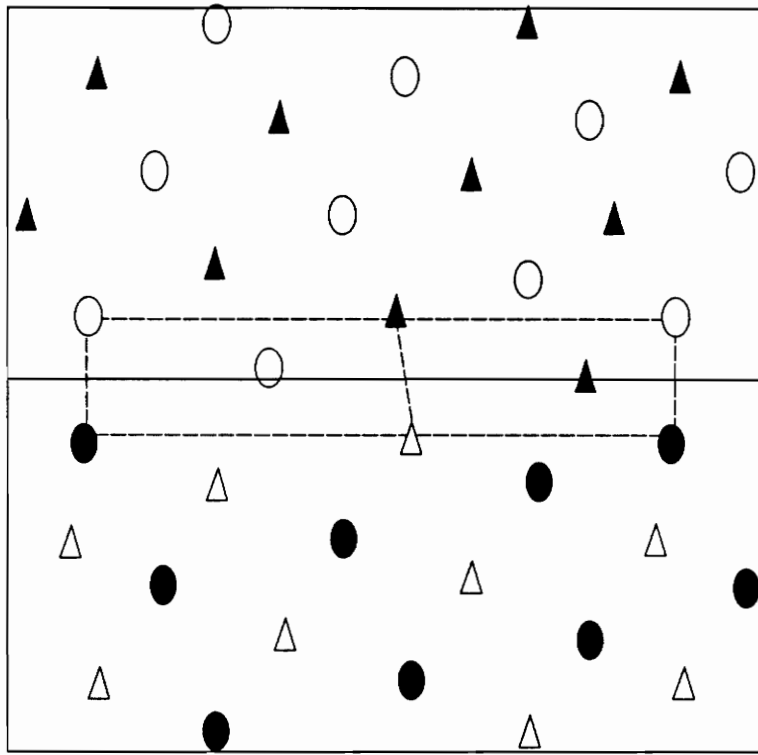


Figure 39. Stoichiometric $\Sigma = 5(310)$ grain boundary structure
 +0.65 Å shift, 909 mJ/m² grain boundary energy

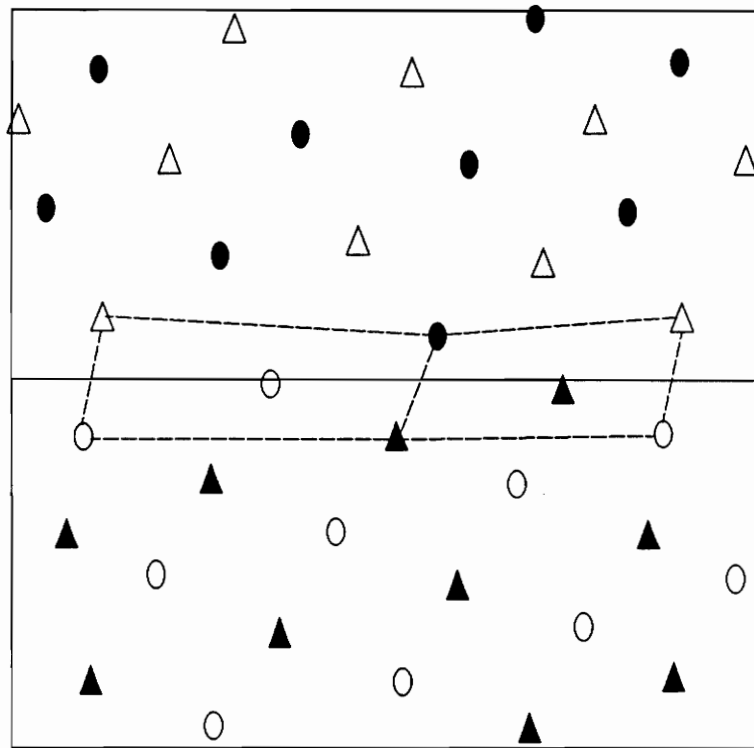


Figure 40. Stoichiometric $\Sigma = 5(310)$ grain boundary structure
 +0.85 Å shift, 896 mJ/m² grain boundary energy

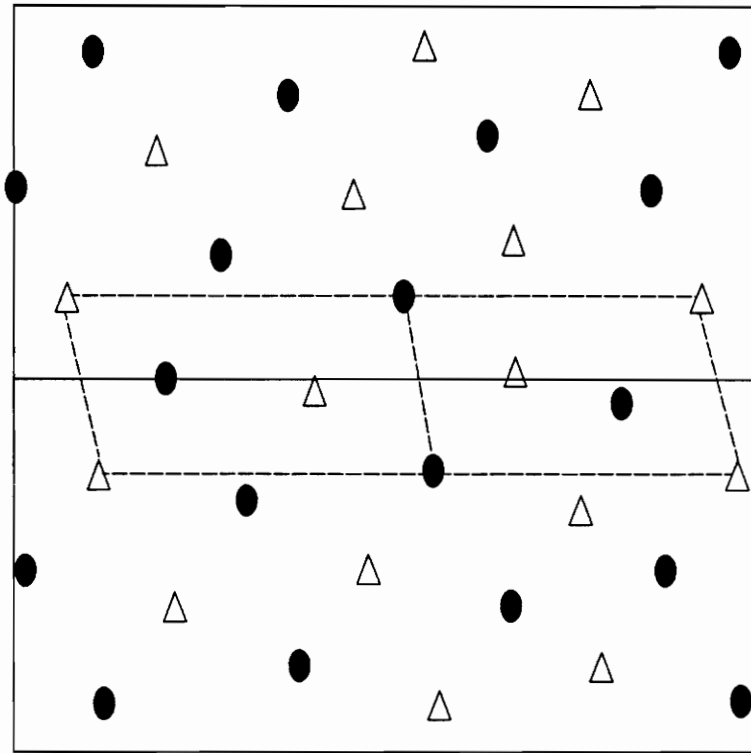


Figure 41.

Stoichiometric $\Sigma = 5(310)$ grain boundary structure

-0.09 \AA shift, 888 mJ/m^2 grain boundary energy

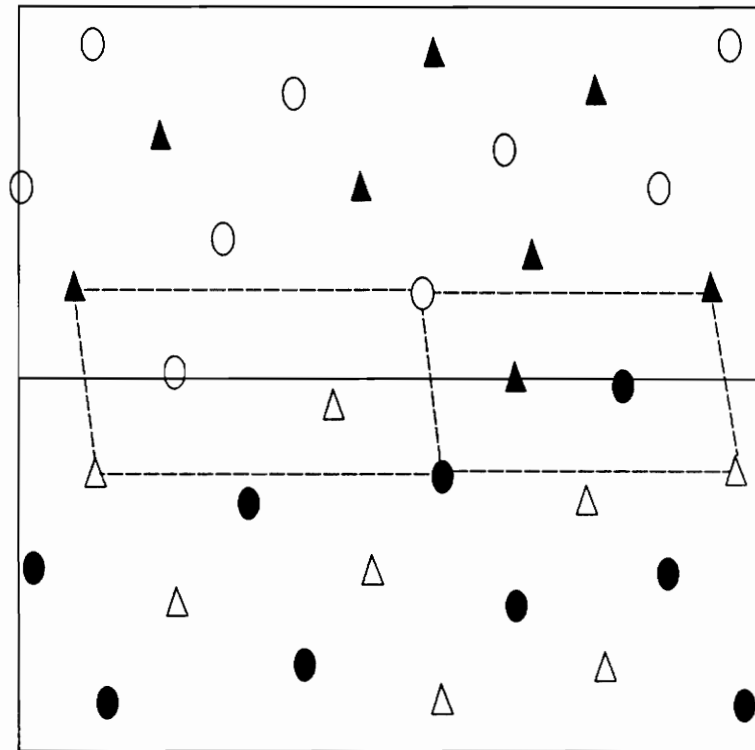


Figure 42. Stoichiometric $\Sigma = 5(310)$ grain boundary structure
 -0.05 \AA shift, $1,336 \text{ mJ/m}^2$ grain boundary energy

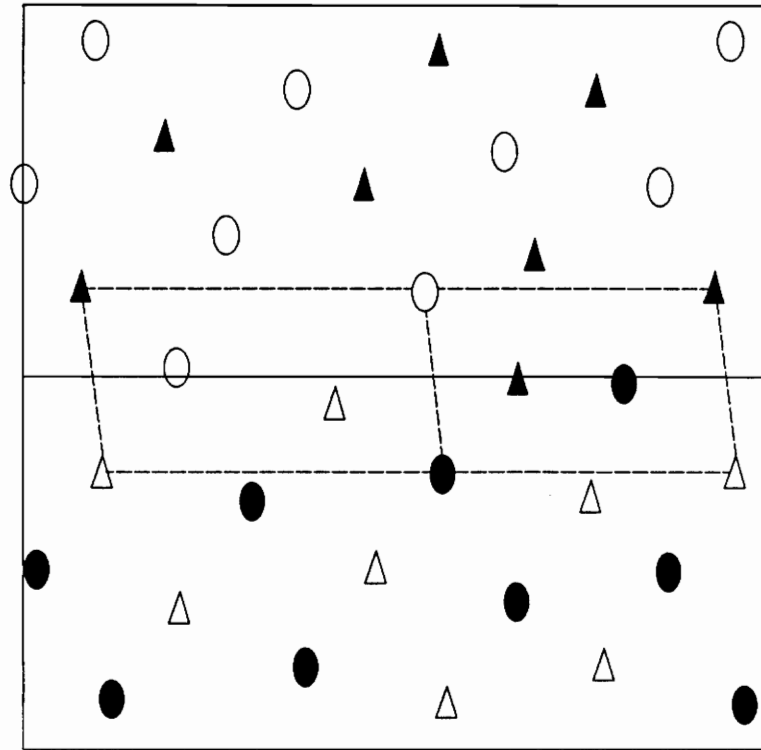


Figure 43. Stoichiometric $\Sigma = 5(310)$ grain boundary structure
-0.10 Å shift, 1,053 mJ/m² grain boundary energy

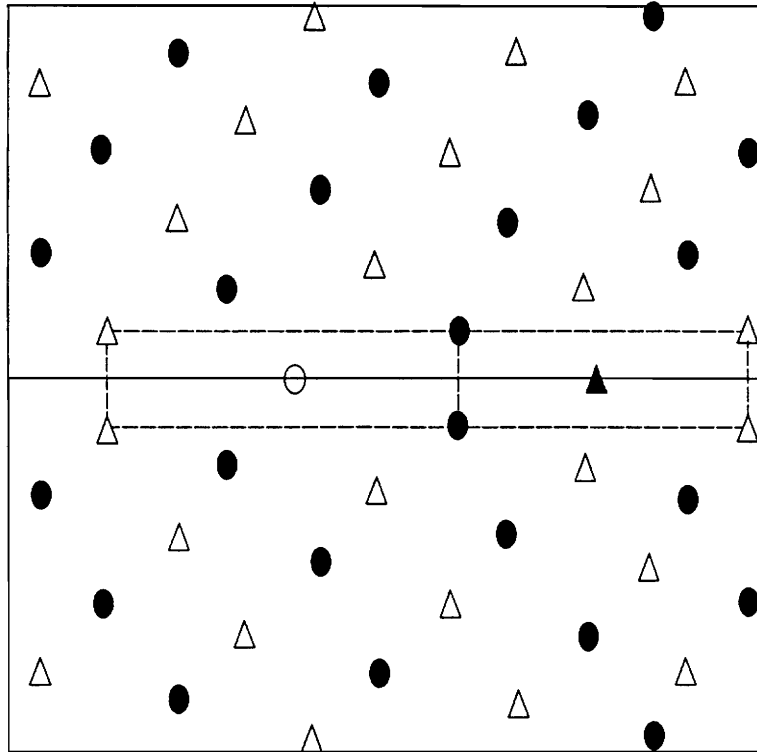


Figure 44. Stoichiometric $\Sigma = 5(310)$ grain boundary structure
 +1.25 Å shift, 1,619 mJ/m² grain boundary energy

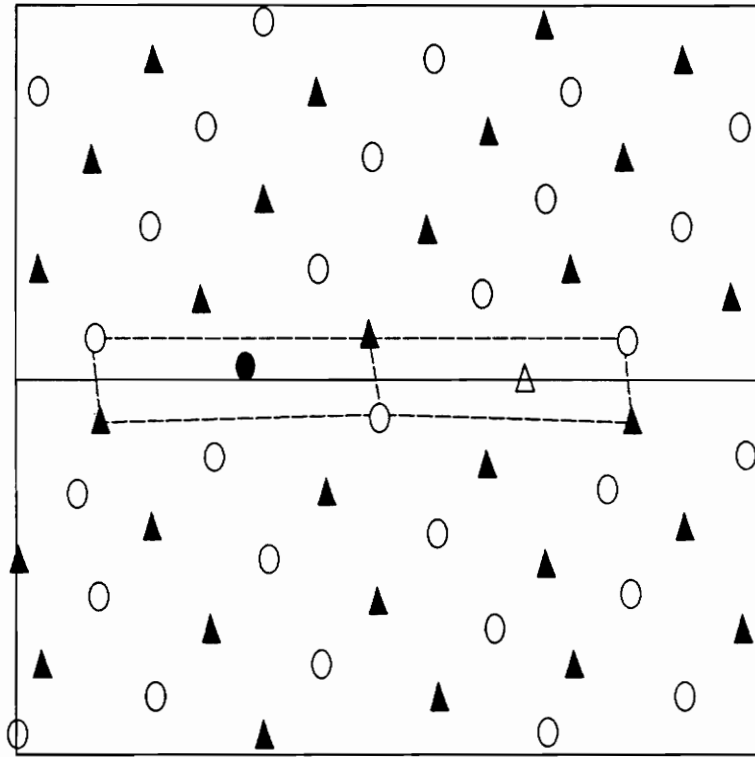


Figure 45. Stoichiometric $\Sigma = 5(310)$ grain boundary structure
 +0.73 Å shift, 1,057 mJ/m² grain boundary energy

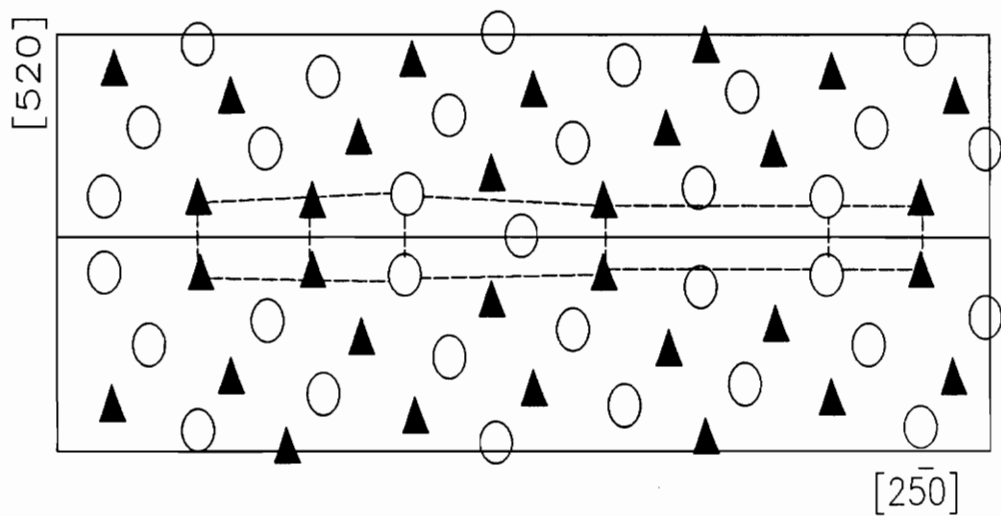


Figure 46. Stoichiometric $\Sigma = 29(520)$ grain boundary structure
 +1.11 Å shift, 1,852 mJ/m² grain boundary energy

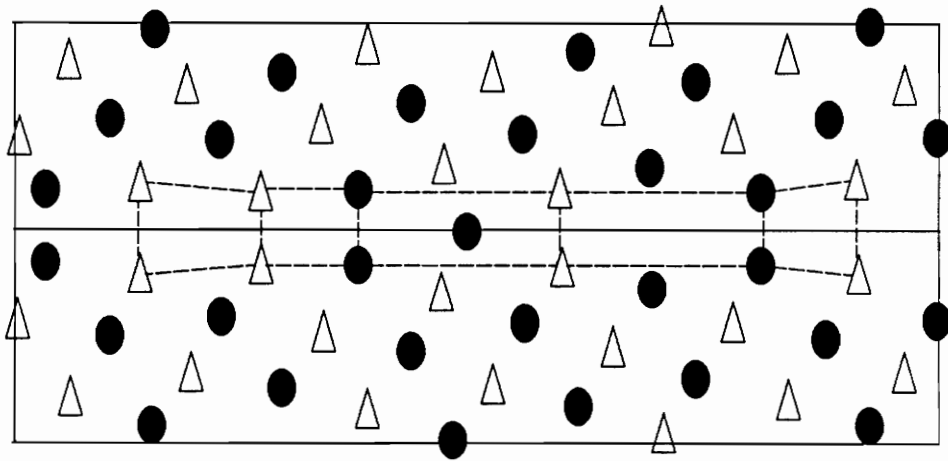


Figure 47. Stoichiometric $\Sigma = 29(520)$ grain boundary structure
+1.27 Å shift, 2,158 mJ/m² grain boundary energy

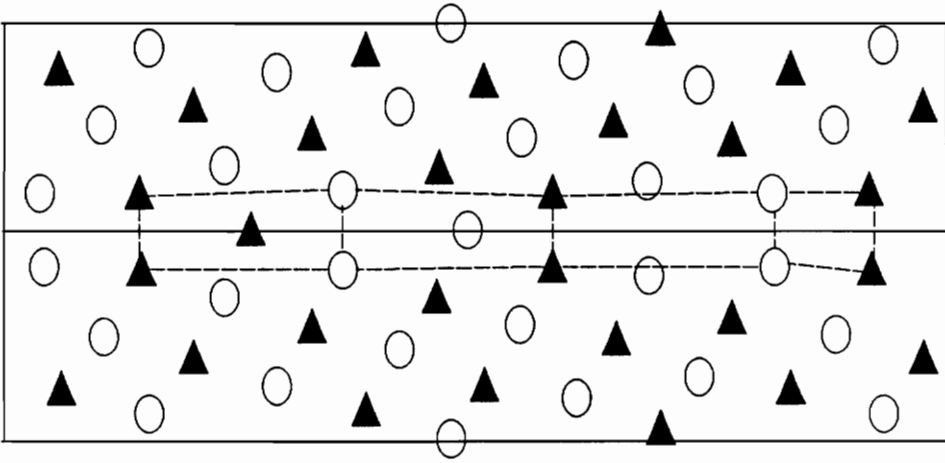


Figure 48.

One excess Al atom $\Sigma = 29(520)$ grain boundary structure
+0.87 Å shift, 1,596 mJ/m² grain boundary energy

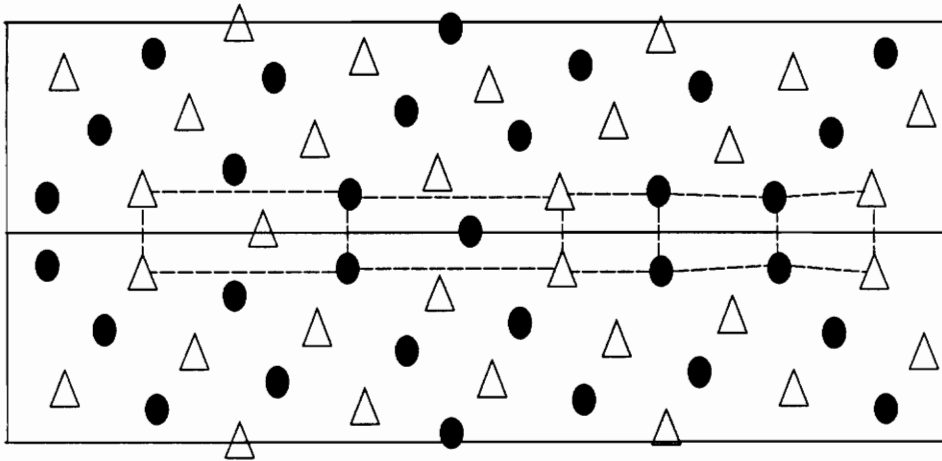


Figure 49.

One excess Ni atom $\Sigma = 29(520)$ grain boundary structure
 +0.52 Å shift, 1,483 mJ/m² grain boundary energy

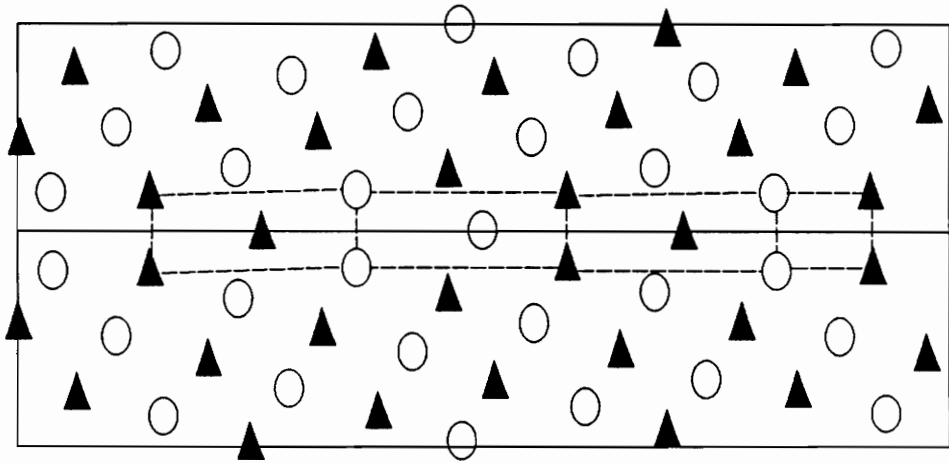


Figure 50. Stoichiometric $\Sigma = 29(520)$ grain boundary structure
 $+0.84 \text{ \AA}$ shift, $1,194 \text{ mJ/m}^2$ grain boundary energy

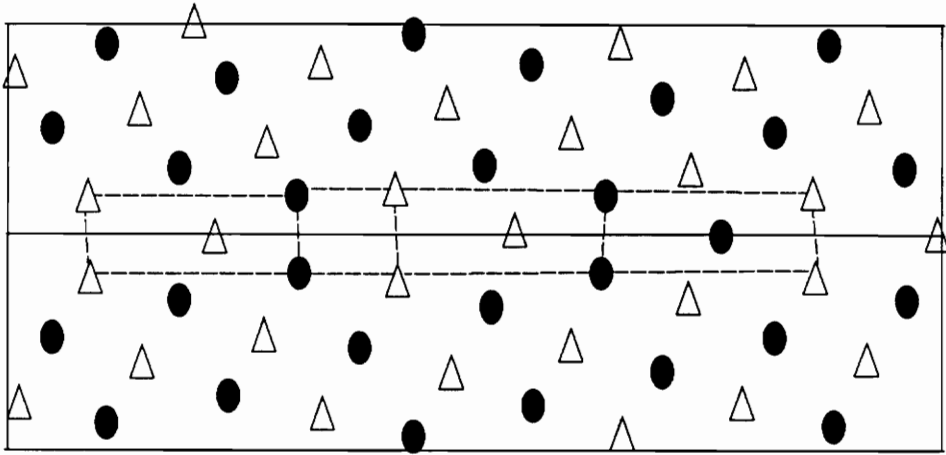


Figure 51. Stoichiometric $\Sigma = 29(520)$ grain boundary structure
+0.75 Å shift, 961 mJ/m² grain boundary energy

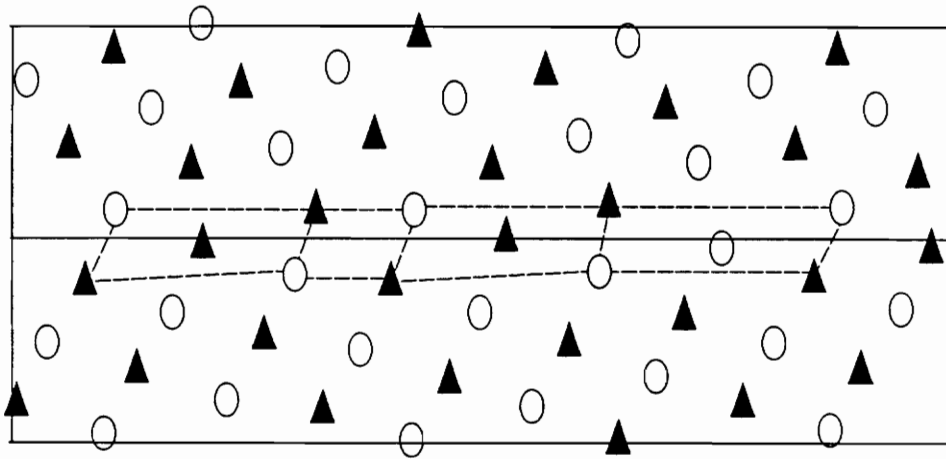


Figure 52. One excess Ni atom $\Sigma = 29(520)$ grain boundary structure
 +0.83 Å shift, 788 mJ/m² grain boundary energy

Figures 50 and 51 show much lower energy structures obtained by adding an atom per structural unit on the grain boundary plane in the structures of Figures 48 and 49. The added atom is nickel type for Figure 50 and aluminum type for Figure 51. Figure 52 is the combination of two configurations of the favored boundaries $\Sigma = 5(210)$ (Figure (15)) and $\Sigma = 5(310)$ (Figure (37)) with low grain boundary energies. The result is a $\Sigma = 29(520)$ boundary with a very low grain boundary energy. The structure in Figure 50 is formed by a combination of structural units in Figures 4 and 38, and in Figure 51 by a combination of those in Figures 5 and 38. This is in agreement with the structural unit model and the energies of the $\Sigma = 29(520)$ boundary are intermediate between those for the favored $\Sigma = 5$ boundaries.

4.1.4 General Results

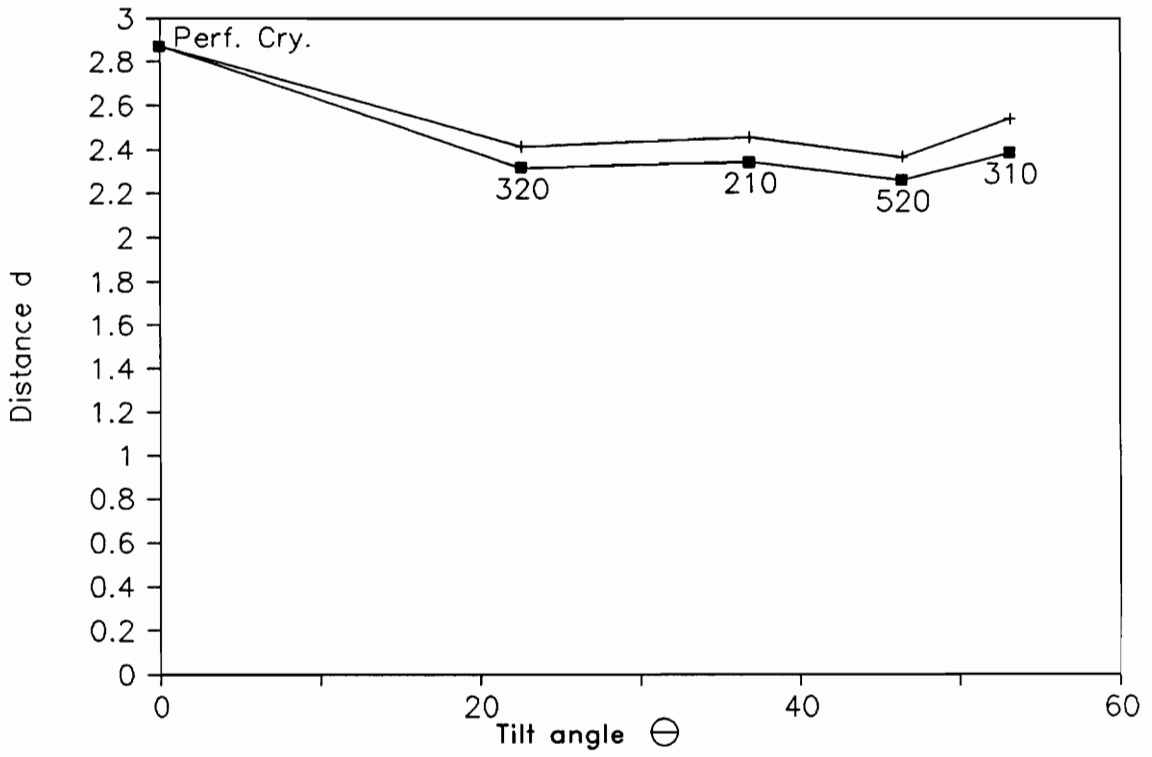
Let us call "d" the distance between the first layers (Figure (4)) for the relaxed structure where no interchanging in atom types, no shift in Z and no removal of layer is made. Figure 53 is the plot of d versus the tilt angle θ . The presence of Ni or Al on the grain boundary plane is a very important factor to take into account. Indeed, this controls whether Al-Al neighbors are found or not. As will be discussed later, Al-Al neighbors play an important role in the grain boundary structure and energy (Table 1).

The equilibrium rigid body translation perpendicular to the boundary plane which corresponds to the volume expansion needed for the minimization of energy, and the grain boundary energy may also be plotted as a function of "d₁" and "d₂" (Figures (54 to 58)). The parameter d₁ is the distance between the nearest layer and the grain boundary for the unrelaxed structure (Figure 54). We considered only the structures for which no layer is removed. Then, when one layer is removed the new parameter is d₂, which is the distance between the second layer and the grain boundary plane, still for the unrelaxed structures (Figure 54). Again, the

Table 1

Distance d between the nearest layers after relaxation for [001] tilt boundaries in the case of no interchanging in atom types, no shift in Z and no layer taken out.

Boundary	Tilt angle θ	d (in Å)	
		Al on grain boundary	Ni on grain boundary
$\Sigma = 5(210)$	36.87 °	2.342	2.458
$\Sigma = 29(520)$	46.40 °	2.261	2.368
$\Sigma = 5(310)$	53.13 °	2.386	2.539



■ Al on the grain boundary plane

+ Ni on the grain boundary plane

Figure 53. d as a function of the tilt angle θ

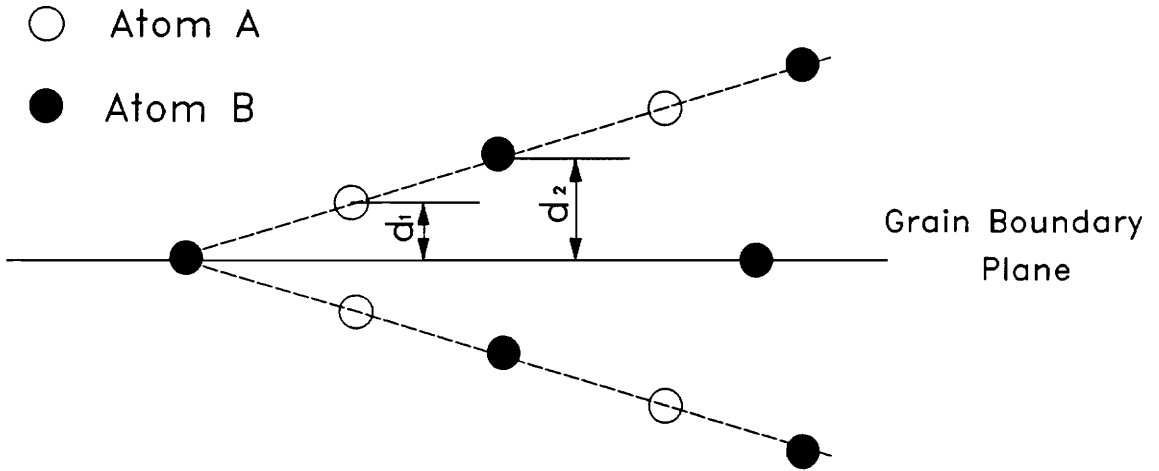
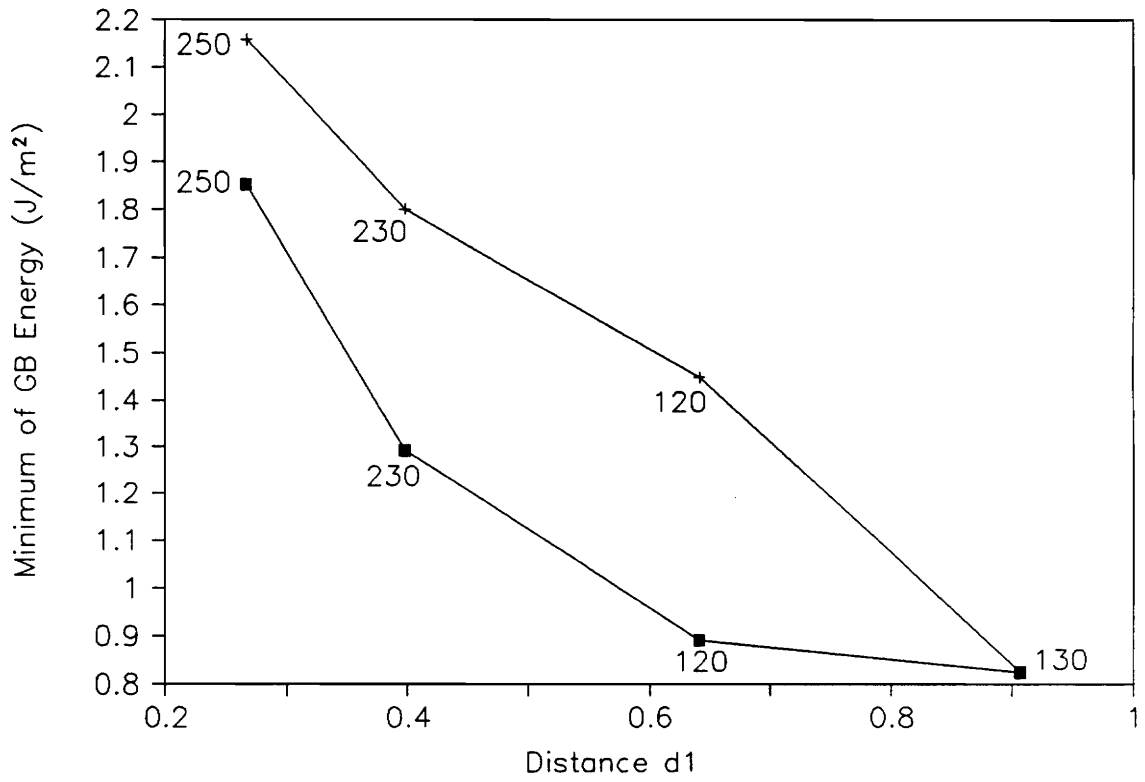


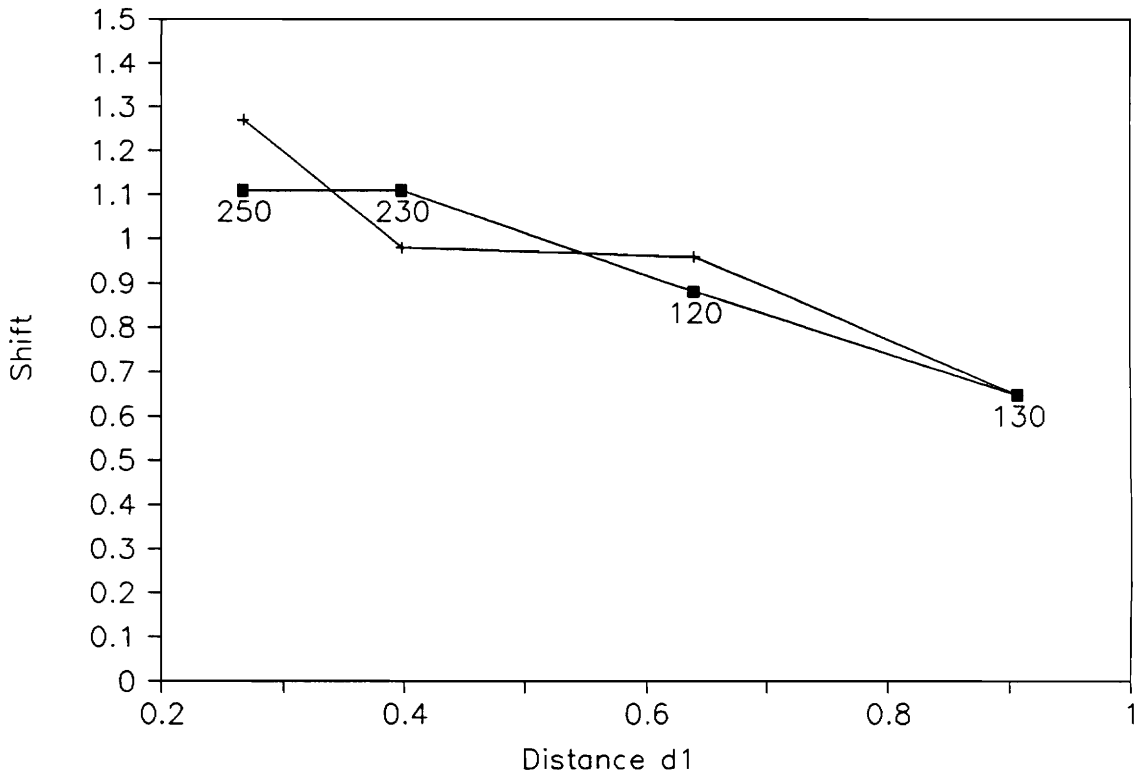
Figure 54. Definition of d_1 and d_2



■ Al on the grain boundary plane

+ Ni on the grain boundary plane

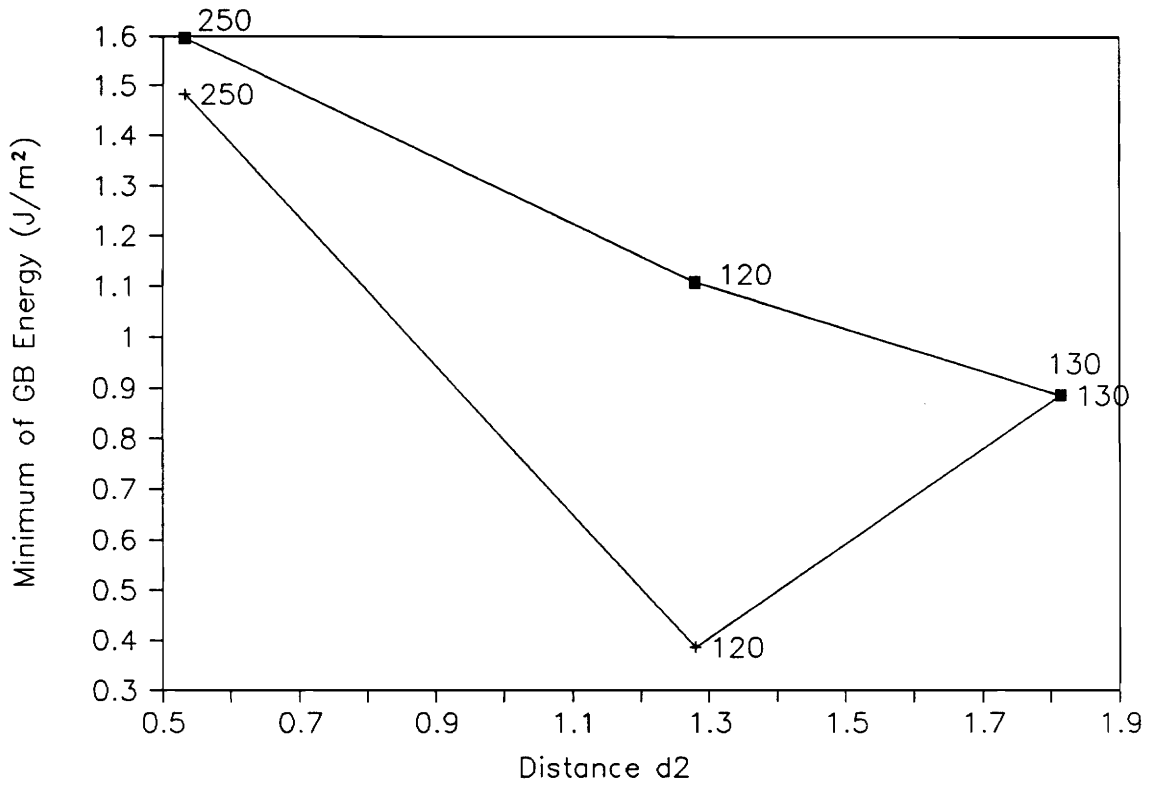
Figure 55. d_1 as a function of the grain boundary energy



■ Al on the grain boundary plane

+ Ni on the grain boundary plane

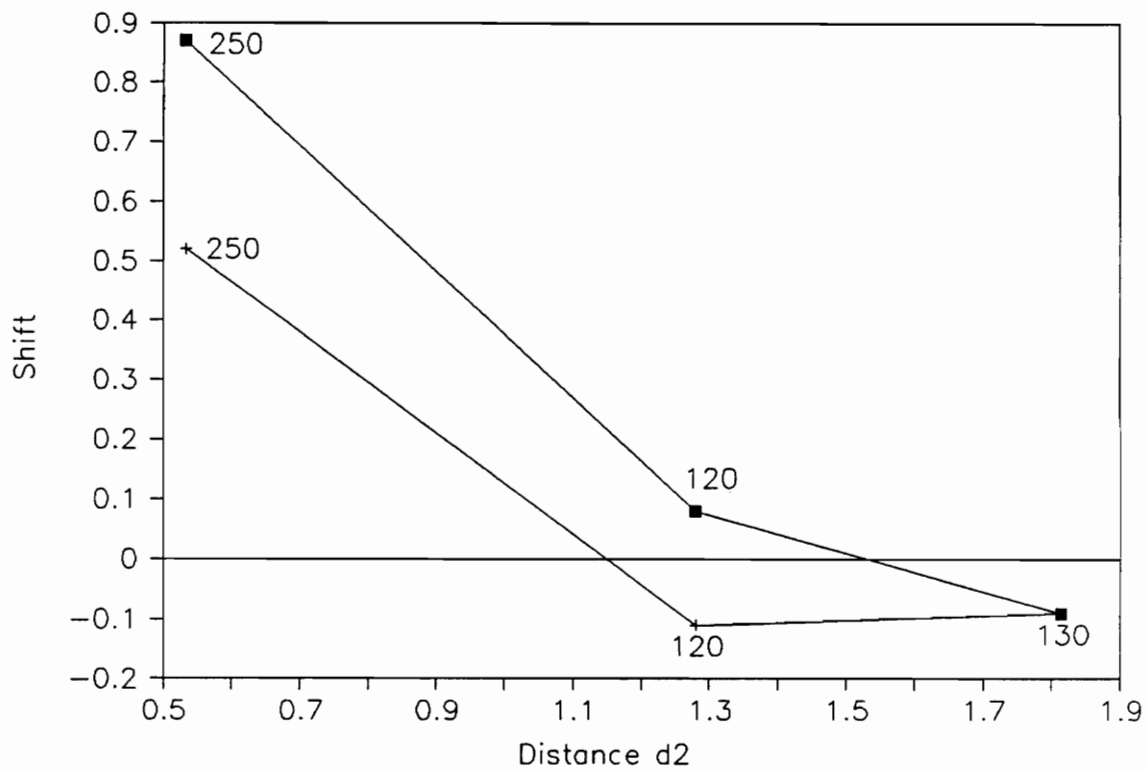
Figure 56. d_1 as a function of the equilibrium shift perpendicular to the grain boundary plane (excess volume)



■ Al on the grain boundary plane
Ni layer taken out

+ Ni on the grain boundary plane
Al layer taken out

Figure 57. d₂ as a function of the grain boundary energy



- Al on the grain boundary plane
Ni layer taken out
- + Ni on the grain boundary plane
Al layer taken out

Figure 58. d_2 as a function of the equilibrium shift perpendicular to the grain boundary plane (excess volume)

presence of aluminum or nickel on the grain boundary has a great influence on the energy and the shift (Table 2 and 3). The excess volumes are larger for boundaries where Al-Al neighbors are present.

4.2 $\Sigma = 3(11\bar{2})[1\bar{1}0]$ Symmetrical Tilt Boundary

Some stoichiometric structures of this boundary are pictured in Figures 59 to 62. A recent work presented this boundary as having no large interstitial holes in the structural unit in Ni₃Al L1₂ structure [29], and it was also shown that cracks try to avoid these boundaries during the fracture process [10,11]. In the case of NiAl B2 phase, the relaxed structures appear to have no large holes either (Figures 59 and 60). In Figures 61 and 62 the structural unit is not symmetrical and the grain boundary energy is very high. This is understandable as many atoms laying in the same $(1\bar{1}0)$ plane, come too close to one another. The shift in Z applied in Figures 61 and 62 is now $\frac{1}{2}\sqrt{2}\alpha_0$.

Table 2

Distance d_1 between the grain boundary and the next nearest layer before relaxation, and the rigid body translation perpendicular to the grain boundary plane (excess volume) and the grain boundary energy in the case of no interchanging in atom types, no shift in Z and no layer taken out.

Boundary	d_1 (in Å)	Equilibrium shift (in Å) perpendicular to the grain boundary plane		Grain boundary energy (in mJ/m ²)	
		Al on grain boundary	Ni on grain boundary	Al on grain boundary	Ni on grain boundary
$\Sigma = 5(210)$	0.641	0.88	0.96	892	1,448
$\Sigma = 29(520)$	0.267	1.11	1.27	1,852	2,158
$\Sigma = 5(310)$	0.907	0.65	0.65	825	825

Table 3

Distance d_2 between the grain boundary and the next nearest layer before relaxation, and the rigid body translation perpendicular to the grain boundary plane (excess volume) and the grain boundary energy in the case of no interchanging in atom types, no shift in Z and the first layer taken out.

Boundary	d_2 (in Å)	Equilibrium shift (in Å) perpendicular to the grain boundary plane		Grain boundary energy (in mJ/m ²)	
		Al on grain boundary	Ni on grain boundary	Al on grain boundary	Ni on grain boundary
$\Sigma = 5(210)$	1.280	0.08	-0.11	1,108	386
$\Sigma = 29(520)$	0.533	0.87	0.52	1,596	1,483
$\Sigma = 5(310)$	1.815	-0.09	-0.09	888	888

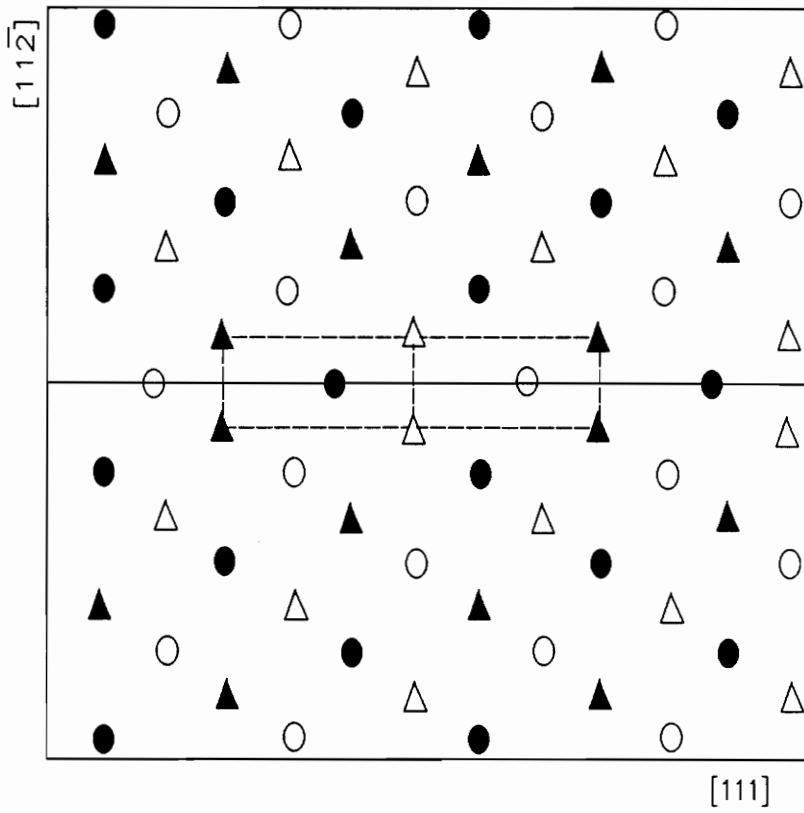


Figure 59.

Stoichiometric $\Sigma = 3(1\ 1\ \bar{2})$ grain boundary structure

0.29 Å shift, 276 mJ/m² grain boundary energy

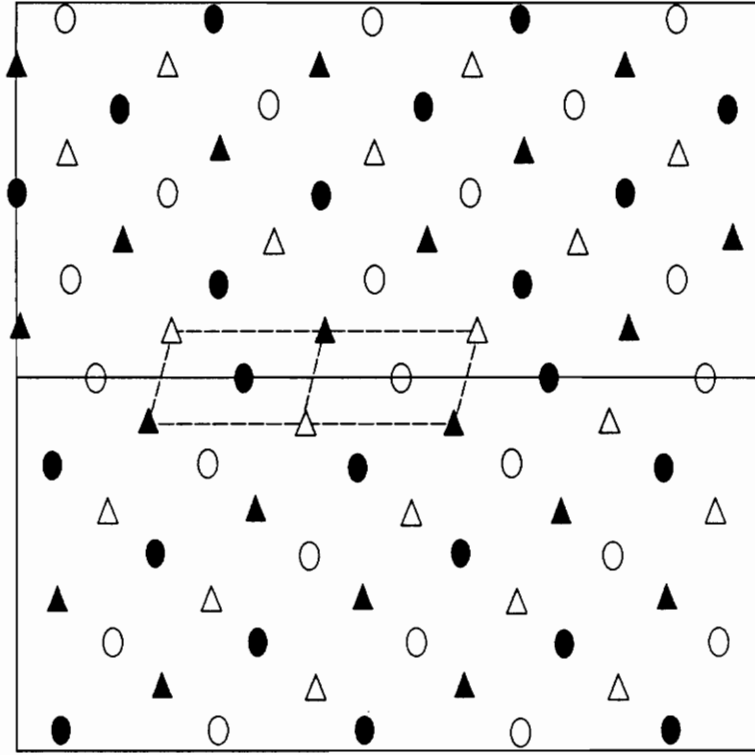


Figure 60. Stoichiometric $\Sigma = 3(11\bar{2})$ grain boundary structure
 0.29 Å shift, 311 mJ/m² grain boundary energy

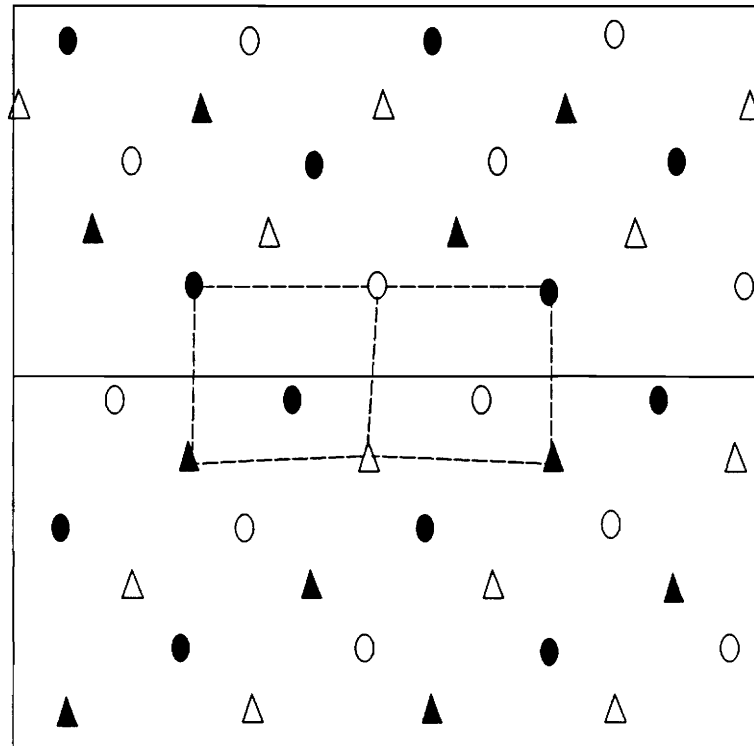


Figure 61. Stoichiometric $\Sigma = 3(11\bar{2})$ grain boundary structure
 1.05 Å shift, 1,739 mJ/m² grain boundary energy

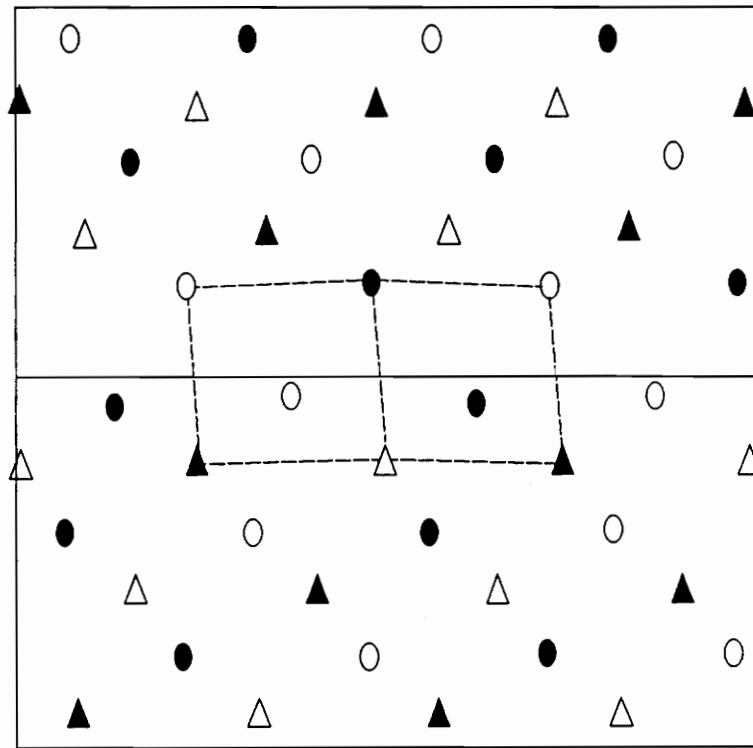


Figure 62.

Stoichiometric $\Sigma = 3(11\bar{2})$ grain boundary structure

1.06 Å shift, 1,975 mJ/m² grain boundary energy

5 DISCUSSION

The first point to be made is that the present analysis shows a trend for the $\Sigma = 5(210)[001]$ tilt boundary energy to be related to the grain boundary stoichiometry (Figure (36)). As we can see on Figure 36, if the Al content increases in the grain boundary the grain boundary energy increases too. This is in agreement with previous observations made on Ni_3Al [30,31]. Therefore, this trend seems to be general of grain boundaries for Al-Ni alloys. Indeed, $\Sigma = 29(520)$ confirms the trend as we observe the energy of one Ni atom rich structure in Figure 52 being lower than the two stoichiometric ones in Figures 50 and 51. This general rule may prove very useful for predicting the range of the energy for unknown boundaries. Note that general trends have to be taken with great care since they are not a strict rule. Figure 36 shows, for example, that energies of one Ni atom rich structures (-1 excess in aluminum) are lower than energies for one Al atom rich structures, but also that they can be much higher than

energies for stoichiometric boundaries. In average one Ni atom rich boundaries lead generally to lower grain boundary energies. Experimental work on NiAl B2 structure [2], has proved the stoichiometric influence on yield strength and ductility.

In Figures 14, 21, 30 and 35, each time two atoms on the grain boundary are located on the same (001) plane, very high energy is obtained (see Figure (63a)). The structure of Figure 14 which has an energy of $1,661 \text{ J/m}^2$ is very close to either the structure of Figure 10 (910 J/m^2) or the one of Figure 11 (746 J/m^2). The same observation may be made between structures in Figures 21 ($1,108 \text{ J/m}^2$) and 20 (936 J/m^2), and also Figures 30 ($1,607 \text{ J/m}^2$) and 29 ($1,308 \text{ J/m}^2$). However the most significant change is between structures of Figure 35 ($1,137 \text{ J/m}^2$) and 33 (342 J/m^2). Thus, the position of the atoms inside the structural plays an important role on the grain boundary energy.

Shifting the atoms on the grain boundary plane by $1/2a_0$ in the Z direction leads also to a dramatic change in the energy (see Figure (63b)). The structure in Figure 8 ($1,713 \text{ J/m}^2$) shifted from the one in Figure 4 ($1,448 \text{ J/m}^2$) is a good example. The same trend is seen for structure 9 ($1,483 \text{ J/m}^2$) shifted from structure 5 (892 J/m^2), and for structure 13 ($1,221 \text{ J/m}^2$) from structure 12 (899 J/m^2). For non stoichiometric boundaries the same thing happens as structure 19 (971 J/m^2) is shifted from structure 18 (386 J/m^2) and structure 28 ($1,357 \text{ J/m}^2$) from structure 27 ($1,108 \text{ J/m}^2$).

The importance of the number of Al-Al neighbors in the boundary has also to be pointed out. Boundaries with low energy seem to be those which tend to minimize Al-Al neighbors (Figure 11 and 18). Also, Al-Al neighbors appear in high energy boundaries such as in the structures of Figures 4 and 25. The $\Sigma = 29(520)$ boundary confirms this particularity. Both structures in Figures 48 and 49 are stoichiometric $\Sigma = 29(520)$ boundaries, nevertheless the structure in Figure 48 which has a higher grain boundary energy than the structure in Figure 49, contains more Al-Al neighbors too. But again, this is not a strict rule. Although they contain Al-Al neighbors, structures in Figures 7, 22 and 27 exhibit relatively low energies. This is probably related to the Al-Al bond distance.

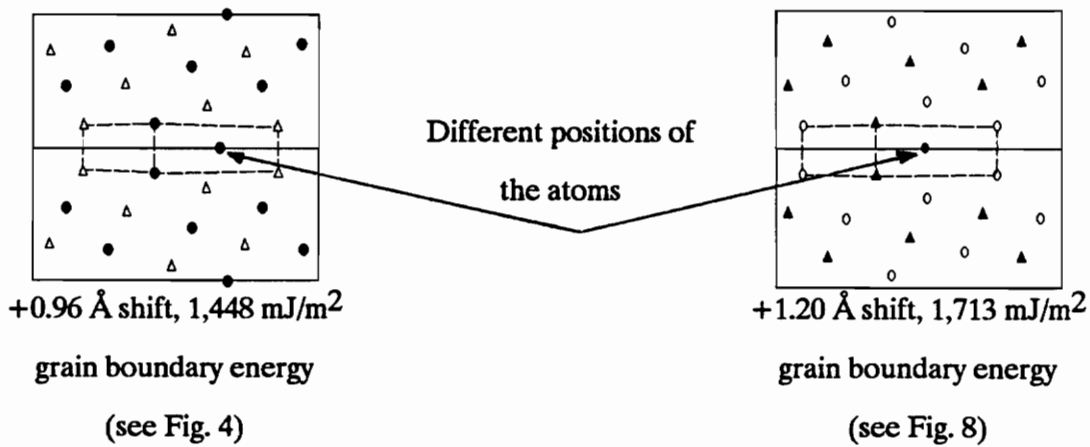


Figure 63a.

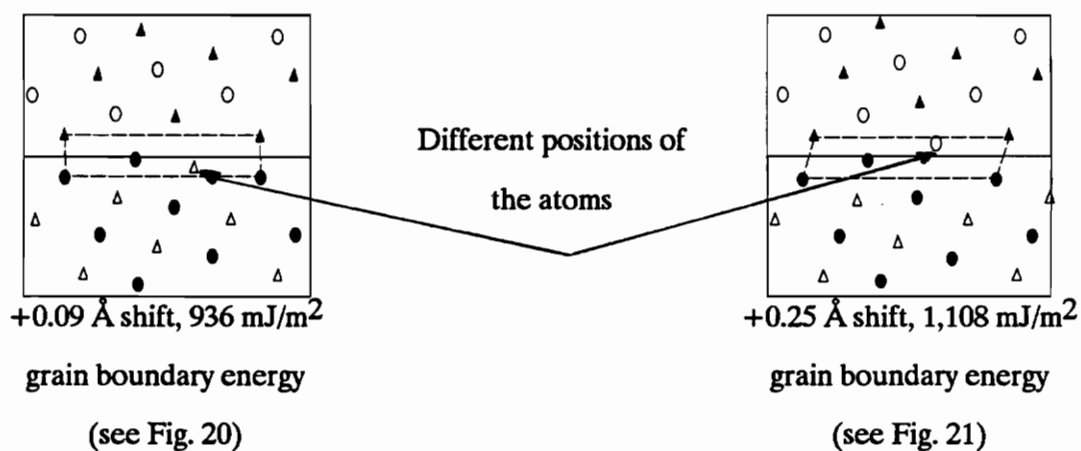


Figure 63b.

Figure 63. Influence of the position of the atoms in the structural unit
 $\Sigma = 5(210)$ grain boundary structures

If we consider d_1 the distance between the first layer and the grain boundary for the unrelaxed structure (Figure (52)), it seems that the grain boundary energy and the shift increase as d_1 decreases (Figures 53 and 54). In these Figures only the basic structures with no shift in Z or interchange of atom types are included in order to be able to make comparisons. So, as the unrelaxed boundary appears to be "more dense" a bigger shift is needed and a higher energy is obtained.

As a result of this (Figure 53), the distance between the two nearest layers for the relaxed structure (d) (see also Figure 4 and Table 1), is independent of the misorientation. This result is in complete agreement with the case of the $L1_2$ structure of the Ni_3Al compound [31]. The distance d is only considered for the basic structures which mean no interchanging in atom types no shift in Z and no layer taken out. The $\Sigma = 5(310)$ boundary is a very special one due to the symmetrical role plaid by nickel and aluminum. For the value of d in the the case of "nickel on the grain boundary" the distance between the two first aluminum layers is taken. In the opposite, case "aluminum on the grain boundary", d is the distance between the two first nickel layers.

In tables 1, 2 and 3 we see that there is a general trend of higher grain boundary energies for larger values of the equilibrium shift perpendicular to the grain boundary plane (excess volume). However, it is also evident that the atom type on the grain boundary plane plays an important role in the grain boundary plane. The reason is that for example if a nickel layer is found on the grain boundary the nearest layers to the interface are aluminum. As we have already discussed Al-Al neighbors bring about a higher energy. Now, we see that it also leads to a higher shift. This trend is verified when an atomic layer is removed. As a matter of fact, if before removal d_1 was considered for two aluminum layers, after the removal of one of these layers, d_2 (Figure (52)) becomes the distance between two nickel layers. So, Al-Al neighbors are changed in Ni-Ni neighbors. this is consistent with the results of Figures 55 and 56. The nickel on the grain boundary energy curves which correspond now to Ni-Ni neighbors

remain lower than the ones for aluminum on the grain boundary. Of course, this is valid only for constant stoichiometry. In the case of a removal of an atomic layer the stoichiometry does change.

Let us consider that one Ni atom rich, one Al atom rich, and stoichiometric structures belong to three different categories. Without looking at the atom type but only to the position of the atoms in the boundary, in each category the lowest energy structure is the same. Structure in Figure 11 is the lowest energy configuration for the stoichiometric $\Sigma = 5(210)$ boundaries. It is similar to the structures in Figure 18 and 27 which are the configurations of lowest energy for the one Ni atom rich and one Al atom rich $\Sigma = 5(210)$ boundaries respectively. And, even when atom types are interverted in this low energy configuration, the new structure remain of moderate grain boundary energy. Figure 10 is an example for stoichiometric boundaries, Figure 22 and 28 for one Ni atom rich and one Al atom rich structures. However no special structure was noticed for being the highest energy configuration in each category. Structures of Figures 14, 21, 30 and 35 where atoms on the interface belong to the same (001) plane have always high grain boundary energy according to the stoichiometry.

The $\Sigma = 3(11\bar{2})[1\bar{1}0]$ tilt boundary exhibits the same properties as the other $[001]$ tilt boundaries. As a matter of fact, structures in Figures 59 and 60 are strictly symmetrical about the boundary plane and yield low energies. Figures 61 and 62 are structures obtained with a shift in Z. This operation brings the atoms of the boundary plane and the ones of the nearest parallel plane in the same $(1\bar{1}0)$ plane. As a result, the energies of these structures have to be relatively high.

We can summarize the parameters which play an important role on the values of grain boundary energies as below :

- * The grain boundary stoichiometry per structural unit.

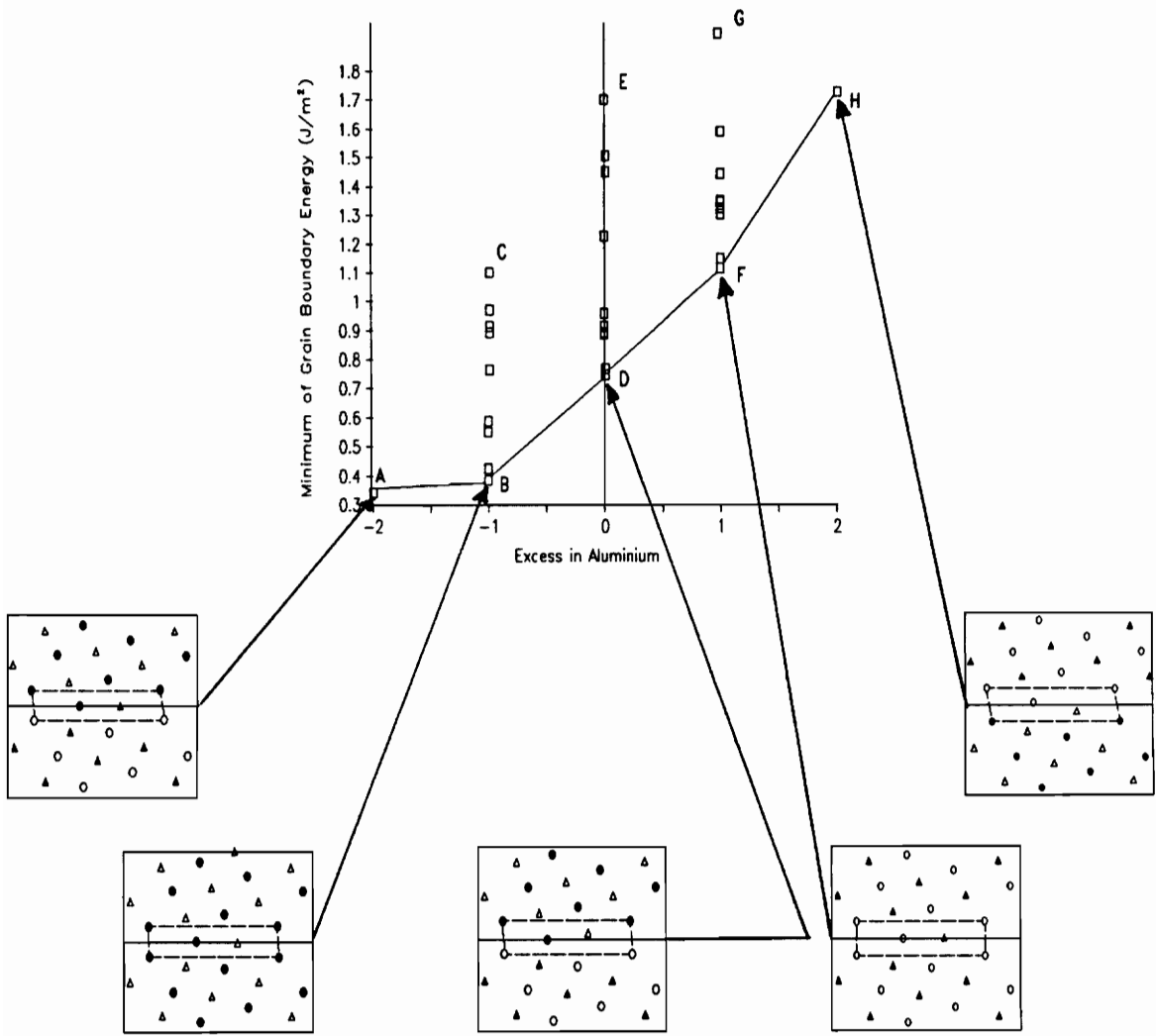
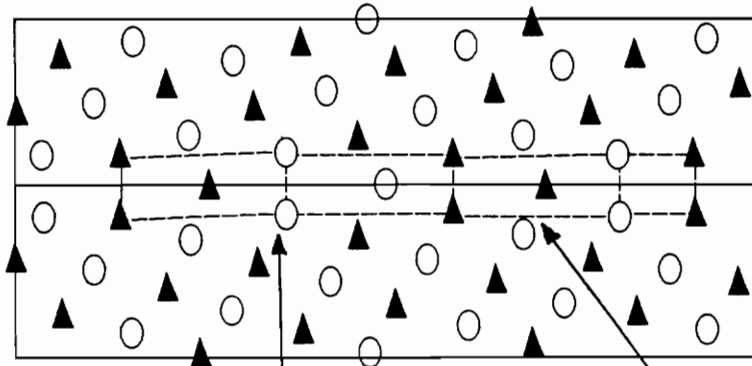


Figure 64. Configuration of lowest energy for $\Sigma = 5(210)$ grain boundary structures

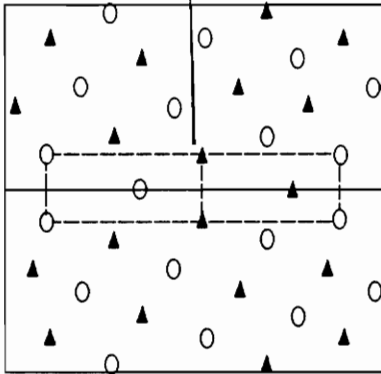
- * The excess volume which correspond to the equilibrium shift perpendicular to the grain boundary. It is also related to the "density" (low values of d_1 or d_2) of the unrelaxed structure.
- * The presence of Al-Al neighbors which is related to the type of atom in the grain boundary plane.
- * The position of the atoms within the structural units.

For non-favored boundaries we can use the fact that some structural units of grain boundary structures are retrieved in others. This is the case for the non-favored $\Sigma = 29(520)$ boundary whose structural unit (Figure 50, 51 and 52) includes the ones of $\Sigma = 5(210)$ and $\Sigma = 5(310)$ favored boundaries (see Figures 65, 66 and 67). It seems that the resulting energy of the non-favored boundary is an average of the two favored boundary energies. If the energies are pretty much the same such as in Figures 5 and 38 the resulting energy has to be a little bit higher (Figure (51)). This is understandable as the two favored structures have to match together bringing more constraints to the system. But, when the energies are very different such as in Figures 4, 38, and 15 and 37, the final energies become moderate (Figures 50 and 51), again according to the stoichiometry.

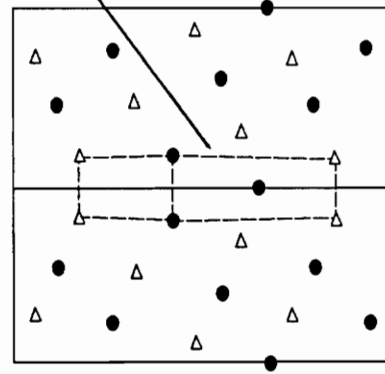
In general, the structural units of the grain boundaries are symmetrical about the grain boundary plane. No large interstitial holes appear in the boundaries. Structures in Figures 4 and 5 exhibit a strict symmetry about the boundary plane. But, even when the symmetry of the unrelaxed structure is broken, symmetry is kept. In Figures 10 and 11 the structures were obtained by removing an atomic layer parallel to the grain boundary. Thus, although the unrelaxed structures were asymmetric, during the relaxation process the symmetry was recovered. This behavior is unlike the results observed for the $\text{Ni}_3\text{AlL}_{12}$ compound. Large interstitial



$\Sigma = 29(520)$
 non-favored boundary
 +0.84 Å shift, 1,194 mJ/m²
 grain boundary energy
 (see Fig. 50)

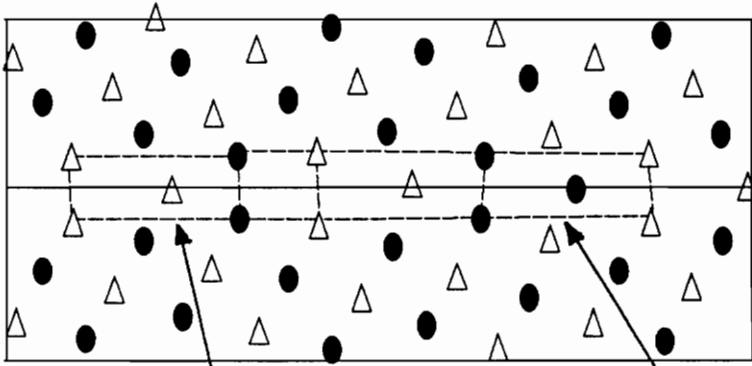


$\Sigma = 5(310)$ favored boundary
 +0.65 Å shift, 825 mJ/m² grain boundary
 energy
 (see Fig. 38)

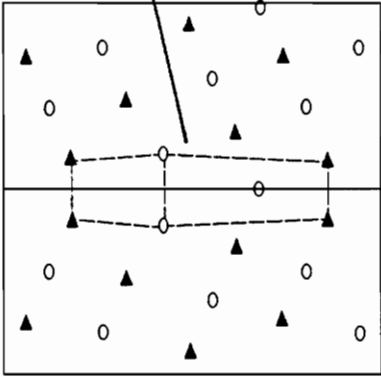


$\Sigma = 5(210)$ favored boundary
 +0.96 Å shift, 1,448 mJ/m² grain boundary
 energy
 (see Fig. 4)

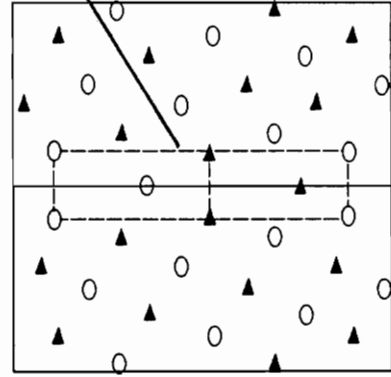
Figure 65. Features of the favored boundaries



$\Sigma = 29(520)$
 non-favored boundary
 +0.75 Å shift, 961 mJ/m²
 grain boundary energy
 (see Fig. 51)

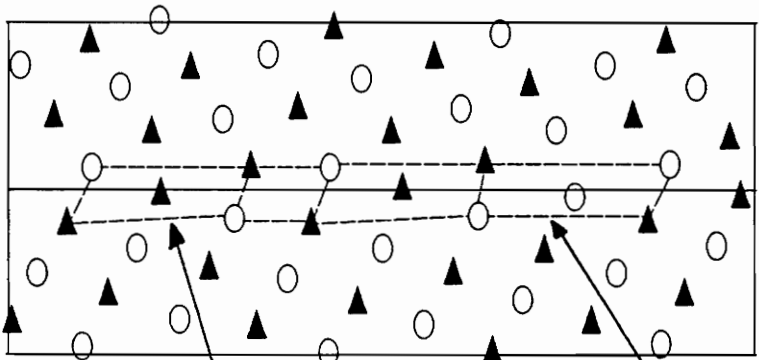


$\Sigma = 5(210)$ favored boundary
 +0.88 Å shift, 892 mJ/m² grain boundary
 energy
 (see Fig. 5)

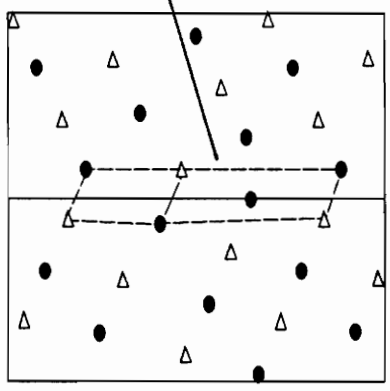


$\Sigma = 5(310)$ favored boundary
 +0.65 Å shift, 825 mJ/m² grain boundary
 energy
 (see Fig. 38)

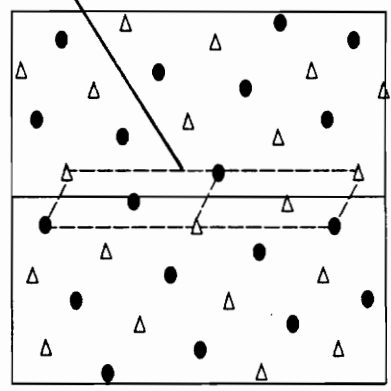
Figure 66. Features of the favored boundaries



$\Sigma = 29(520)$
 non-favored boundary
 +0.83 Å shift, 788 mJ/m²
 grain boundary energy
 (see Fig. 52)



$\Sigma = 5(310)$ favored boundary
 +0.61 Å shift, 427 mJ/m² grain boundary
 energy
 (see Fig. 15)



$\Sigma = 5(310)$ favored boundary
 +0.73 Å shift, 855 mJ/m² grain boundary
 energy
 (see Fig. 37)

Figure 67. Features of the favored boundaries

holes in Ni₃Al grain boundaries were observed [7], giving a possible interpretation of the intrinsic brittleness of the Ni-Al alloys. The holes were said to induce micro-cracks in the boundaries, responsible for brittleness. This explanation can not be applied to NiAl B2 phase since no large interstitial holes were found. The intergranular brittleness could have come from environmental effects, such as segregation at the grain boundaries. However, polycrystalline NiAl B2 phase was recently found to be intrinsically brittle by George and Liu [32].

An alternate explanation for the grain boundary brittleness is needed. A possible explanation could be that under stress, dislocations arriving at the boundary may change low energy boundary structures to high energy ones. Indeed, the difference in energy among the different structures are quite large and dislocation motion may be obtained according to the ductility of the NiAl single crystal. According to the type of dislocation and the initial boundary structure, the final structure may vary. The dislocation line would act as a limit among two possible grain boundary structures. Therefore, it seems that some of the high energy structures actually could appear when the material is subject to stresses which induce dislocation motion. These high energy structures can significantly affect the deformation process, and may be an important factor in the mechanical behavior of the boundaries. This is the alternate explanation of grain boundary brittleness that we propose here and we believe needs to be explored further.

6 CONCLUSIONS

The results indicate clearly that the stoichiometry of the grain boundary has an influence on the grain boundary energy. The higher the aluminum content, the higher the grain boundary energy and as a result the more brittle the material. This result agrees with previous work on Ni₃Al [30,31].

Some structures appear to give high grain boundary energies for all stoichiometries. When atoms on the boundary plane lay within the same (001) plane for [001] tilt boundaries, the energy is always high. In the case of $\Sigma = 3(11\bar{2})[1\bar{1}0]$ tilt boundary, high energy structures appear when atoms of the boundary plane and of a nearest parallel plane to the grain boundary lay within the same $(1\bar{1}0)$ plane. For this case, atoms on the boundary plane are within the same $(1\bar{1}0)$ plane.

A shift in the Z direction of atoms on the boundary plane, also brings high energy structures. Structures with Al-Al neighbors exhibit high grain boundary energy. As a matter of fact, it seems that the more Al-Al neighbors, the higher the energy. As the distance between the boundary plane and the first parallel layer for the unrelaxed structure (d_1 or d_2) decreases the energy and the shift increase. When Σ gets high, the probability to get a low d_1 or d_2 increases. This is in agreement with the fact that high Σ structures usually have a high grain boundary energy.

The same structure was found to be the lowest for all stoichiometries in the case of $\Sigma = 5(210)$ boundary if the atom type is not considered but only the position of the atoms.

Features of the favored boundaries were retrieved. Indeed, results obtained for the favored boundaries may be used to predict the energy and structures of non-favored boundaries. Indeed, the structure and the range of the energy of the $\Sigma = 29(520)$ boundary fell within the predictions made by using the features of $\Sigma = 5(210)$ and $\Sigma = 5(310)$.

Most structural units are symmetrical about the boundary plane which is unlike the result found for Ni_3Al . The hypothesis that the big interstitial holes enhance micro-crack formation inside the boundary and then make the material intrinsically brittle can not be applied for NiAl B2 phase. Another phenomenon must have interfered. Since it was shown that the grain boundaries in NiAl are intrinsically brittle [32], environmental effects can not be the interpretation, and one explanation could be that the boundary structures are switched to high energy ones as dislocations show up at the boundary.

Finally, as a suggestion for a further study, the dislocation interaction with grain boundaries should be studied. Indeed, the change from low energy boundary structures to high energy ones as the dislocations arrive at the grain boundary was stated as the alternate explanation for intergranular brittleness in NiAl B2 phase. Since all possible structures were found for $\Sigma = 5(210)$ and $\Sigma = 5(310)$ boundaries, the effect of a dislocation crossing the boundary may be observed. By putting a dislocation at different positions relatively to the grain boundary, the switch from one structure to another should be noticed.

7 REFERENCES

- 1 C. T. Liu, C. L. White and J.A. Horton, *Acta Metall.*, **33**, 213, (1985).
- 2 K. H. Hahn and K. Vedula, *Scripta Met.* **23**, 7 (1989).
- 3 A. P. Sutton, and V. Vitek, *Phil. Trans. R. Soc. Lond. A* **309**, 1-36 (1983).
- 4 A. P. Sutton, *International Metals Reviews*, **29**, 377 (1984).
- 5 V. Rangarajan, Master Thesis, Virginia Polytechnic Institute and State University, "A Study of Grain Boundary Structures in Boron doped Ni₃Al" (1986).
- 6 T. Takasugi, N. Masahashi and O. Izumi, *Acta Metall.* **35**, N_O 2, 381 (1987).

- 7 J. Kruisman, V. Vitek and J. Th. M. DeHosson, *Acta Metall.* **36**, 2729 (1988).
- 8 D. Farkas and V. Rangarajan, *Acta Metall.*, **35**, N^o 2, 353 (1987).
- 9 D. Farkas, *MRS Symposia Proceedings*, **"High-Temperature Ordered Inter-metallic Alloys"**, **39**, 133 (1985).
- 10 S. Hanada, T. Ogura, S. Watanabe, O. Izumi and T. Masumoto, *Acta Metall.* **34**, No 1 (1986) 13.
- 11 H. Lin and D. P. Pope, *MRS Spring Meeting 1990*, **"A Study of Intergranular Fracture in Ni₃Al using Electron Backscattering Pattern Method"**, San Francisco.
- 12 A. F. Voter and S. P. Chen, *MRS Symposia Proceedings*, **"Characterization of Defects in Materials"**, **82**, 175 (1987).
- 13 W. Bollmann, **"Crystal Defects and Crystalline Interfaces"**, Springer, Berlin (1970).
- 14 D. Hull, **"Introduction to Dislocations"**, Pergamon Press, (N. Y.), (1975).
- 15 Ho Jang, Thesis, Virginia Polytechnic Institute and State University, **"Grain Boundary Studies in Ordered Intermetallic Compound Ni₃Al"**, (1990).
- 16 G. Hermann, H. Gleiter and G. Bäro, *Acta Metall.* **24**, 353 (1976).
- 17 H. Mykura, P.S. Bansal and M. H. Lewis, *Phil. Mag. A* **42**, 225 (1980).

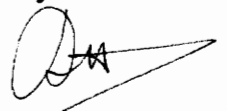
- 18 R. W. Ballufi, A. Brokman and A. H. King, *Acta Metall.* **30**, 1453 (1982).
- 19 A. Brokman and R. W. Ballufi, *Acta Metall.* **29**, 1703 (1981).
- 20 A. A. Maradudin, E. W. Mantroll, G. H. Weiss and I. P. Ipatova, "Theory of Lattice Dynamics in the Harmonic Approximation", *Solid State Physics supplement, V. 3'*, Academic Press. N. Y. (1971).
- 21 PR. Chidambaram, Thesis, Virginia Polytechnic Institute and State University, "Computer Simulation Of Lattice Defects In Ni₃Al", (1987).
- 22 M. J. Norgett, R. C. Perrin, and E. J. Savino, *J. Phys. F* **2**, L 73, (1972).
- 23 I. M. Torrens, "Interatomic Potentials", Academic Press, (N. Y.), (1972).
- 24 E. S. Machlin, *Acta Metall.* **22**, 95, (1974).
- 25 E. S. Machlin, *Acta Metall.* **22**, 109, (1974).
- 26 E. S. Machlin, *Acta Metall.* **22**, 1433, (1974).
- 27 E. J. Savino and D. Farkas, *Phil. Mag. A.* **58**, 227 (1988).
- 28 K. Madea, V. Vitek and A. P. Sutton, *Acta Metall.* **30**, 2001 (1982).
- 29 Jun Liao and Diana Farkas, to be published.
- 30 S. P. Chen, A. F. Voter and D. J. Srolovitz, *Scripta Met.* **20**, 1389 (1986).

- 31 S. P. Chen, A. F. Voter and D. J. Srolovitz, *J. Mat. Research* **4**, 62 (1989).
- 32 E. P. George and C. T. Liu, *J. Mater. Res.*, **5**, No. 4, 754 (1990).

VITA

The author was born on April 4th, 1966 in Douala (Cameroon). As he has the French citizenship, he completed the undergraduate program in Mathematics and Physics in Brest (France). After two years of "Mathématiques Supérieures" and "Mathématiques Spéciales" he entered the engineering school "Ecole Nationale Supérieure d'Arts et Métiers" (E.N.S.A.M.) which leads to a degree in Mechanical Engineering. The first two years of E.N.S.A.M. were in Angers, city where the author met his wife. Then, the graduation year was in Paris. After the graduation in June 1989 the author joined the Department of Materials Engineering, Virginia Polytechnic Institute and State University, for a Master's program. In January 1991 the author will be called for the military service which is mandatory for all young French male. He will do it as a researcher in a German laboratory for Pechiney, a French Company, during 16 months. Then the author will work for the research plant of this company located in Grenoble (France). But the most important, the author will become a daddy in November 1990.

Guy PETTON

A handwritten signature in black ink, consisting of a large, stylized 'G' followed by 'uy' and a long horizontal stroke extending to the right.